nature neuroscience

ARTICLES

https://doi.org/10.1038/s41593-020-00716-1

Synaptic vesicles transiently dock to refill release sites

Grant F. Kusick[1,2], Morven Chin[1,6], Sumana Raychaudhuri[1], Kristina Lippmann[3,7,9], Kadidia P. Adula[3,8,9], Edward J. Hujber[3,4,9], Thien Vu[3,4,9], M. Wayne Davis[4], Erik M. Jorgensen[3,4] and Shigeki Watanabe[1,3,5] ✉

Synaptic vesicles fuse with the plasma membrane to release neurotransmitter following an action potential, after which new vesicles must 'dock' to refill vacated release sites. To capture synaptic vesicle exocytosis at cultured mouse hippocampal synapses, we induced single action potentials by electrical field stimulation, then subjected neurons to high-pressure freezing to examine their morphology by electron microscopy. During synchronous release, multiple vesicles can fuse at a single active zone. Fusions during synchronous release are distributed throughout the active zone, whereas fusions during asynchronous release are biased toward the center of the active zone. After stimulation, the total number of docked vesicles across all synapses decreases by ~40%. Within 14 ms, new vesicles are recruited and fully replenish the docked pool, but this docking is transient and they either undock or fuse within 100 ms. These results demonstrate that the recruitment of synaptic vesicles to release sites is rapid and reversible.

Synaptic vesicle fusion takes place at a specialized membrane domain: the active zone[1]. The active zone is organized into one or more release sites, individual units at which a single synaptic vesicle can fuse[2]. Ultrastructural studies have demonstrated that some synaptic vesicles are in contact with the plasma membrane in the active zone and define the 'docked' pool[3,4]. Since both docking and physiological readiness require engaged SNARE proteins[4–6], docked vesicles are thought to represent fusion-competent vesicles. In fact, previous studies have demonstrated that docked vesicles are partially depleted following stimulation[7–9]. However, it is not clear how release sites are refilled by vesicles to sustain neuronal activity.

The docking of vesicles to refill release sites must be rapid. A single action potential consumes some docked vesicles, whereas bursts of action potentials would be expected to deplete all docked vesicles. Nevertheless, some central synapses can fire at a frequency of 1 kHz[10]. Studies using electrophysiology and electron microscopy indicate that recovery of the docked and readily releasable vesicle pools is slow—about 3 s[7,8,11]. However, an emerging body of work suggests that vesicle replenishment comprises several kinetically and molecularly distinct steps, some of which may occur on very fast timescales. In two notable recent examples, modeling based on physiological data predicted that vesicles reversibly transition from "replacement sites" to "docking sites" within milliseconds of an action potential[12,13], and experiments using flash-and-freeze electron microscopy demonstrated that synaptotagmin-1 mutants with docking defects can be reversed by binding calcium[9]. These fast vesicle docking events have been proposed to correspond to calcium-induced changes between loose and tight assembly of the SNARE complex, which may be both very fast and reversible[14]. However, there is currently no ultrastructural evidence for such fast and reversible docking steps at wild-type synapses.

To characterize the ultrastructure of vesicle docking and fusion at active zones, we developed a method called 'zap-and-freeze' to trigger single action potentials by electrical stimulation followed by high-pressure freezing at defined time points. Using this approach, we first characterized the spatial and temporal organization of fusion sites following a single action potential. We observed that during synchronous release, multiple vesicles can fuse per action potential within the same active zone, even in physiological extracellular [Ca^{2+}]. Fusions during synchronous release occur throughout the active zone, but are concentrated at the center of the active zone during asynchronous release. We then followed the fate of docked vesicles. Unexpectedly, ~40% of docked vesicles are lost immediately after stimulation, which is due to fusion and, potentially, undocking. These are then fully replaced by newly docked vesicles within 14 ms, perhaps to counteract short-term depression. This transient docking requires residual calcium in the terminals and only lasts for 100 ms or less (Extended Data Fig. 1). This sequence of rapid redocking and subsequent slow undocking may underlie facilitation.

Results

Zap-and-freeze captures synaptic vesicle fusion. To capture exocytosis with millisecond precision under physiologically relevant conditions, we developed a system to electrically stimulate neurons before high-pressure freezing. This consisted of a small, portable field-stimulation device with a photoelectric control switch (Fig. 1a). This device can be charged, then loaded into a high-pressure freezer

[1]Department of Cell Biology, Johns Hopkins University, School of Medicine, Baltimore, MD, USA. [2]Biochemistry, Cellular and Molecular Biology Graduate Program, Johns Hopkins University, School of Medicine, Baltimore, MD, USA. [3]Neurobiology Course, The Marine Biological Laboratory, Woods Hole, MA, USA. [4]Department of Biology and Howard Hughes Medical Institute, University of Utah, Salt Lake City, UT, USA. [5]Solomon H. Snyder Department of Neuroscience, Johns Hopkins University, School of Medicine, Baltimore, MD, USA. [6]Present address: Program in Neuroscience, Harvard University, Cambridge, MA, USA. [7]Present address: Carl-Ludwig-Institute for Physiology, University Leipzig, Leipzig, Germany. [8]Present address: Department of Molecular, Cell, and Developmental Biology, University of California, Los Angeles, Los Angeles, CA, USA. [9]These authors contributed equally: Kristina Lippmann, Kadidia P. Adula, Edward J. Hujber and Thien Vu. ✉e-mail: shigeki.watanabe@jhmi.edu

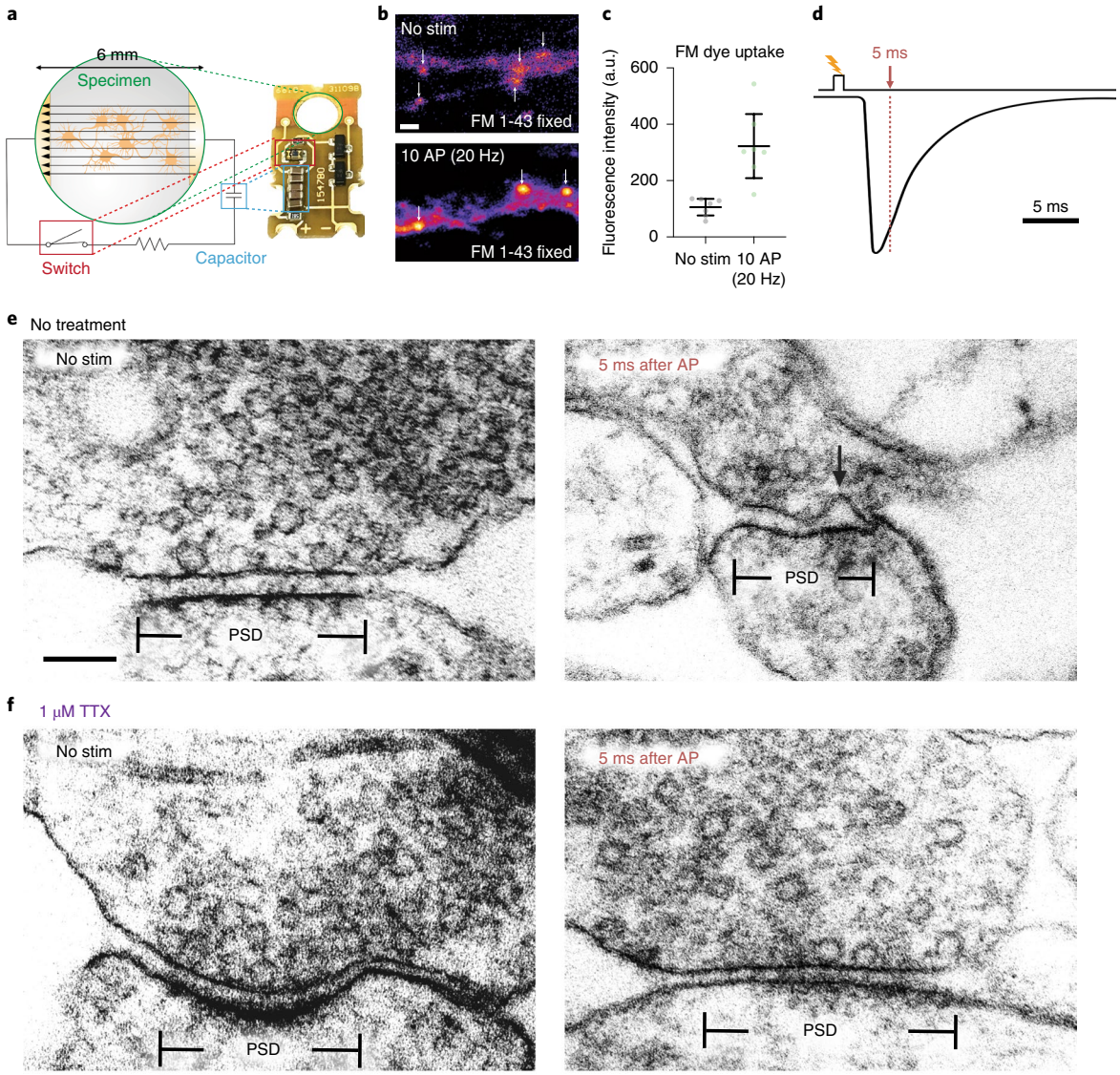

Fig. 1 | Zap-and-freeze captures synaptic vesicle fusion. a, Schematic and photograph of the zap-and-freeze stimulation device. **b**, Epifluorescence micrographs of cultured mouse hippocampal neurons pre-incubated in Pitstop 2 (30 μM) in physiological saline (1 mM Ca^{2+}) for 2 min, then either not stimulated (No stim) or subjected to ten 1-ms pulses at 20 Hz (10 AP) at 37 °C in FM 1-43FX, followed by washing and fixation. Arrows indicate putative presynaptic terminals, which were identified by their increased FM labeling relative to the rest of the axon, shape and size. Scale bar, 2 μm. **c**, Quantification of the experiment described in **b** expressed in arbitrary units (a.u.). $n = 7$ fields of view with 20 total putative boutons quantified per image; $P = 0.003$, two-sided Welch's t-test, $N = 1$ experiment. Note that the images shown in **b** are crops of a small portion of the full field of view for each image. Error bars indicate the mean and 95% confidence interval. **d**, Experimental design for stimulation and freezing, showing a diagrammatic excitatory postsynaptic current for reference (based on ref. [28]). A 1-ms square pulse is applied to trigger a single action potential (AP), then neurons are frozen 5 ms after the beginning of the pulse (this is the earliest possible freezing time on the high-pressure freezer; Methods). **e**,**f**, Transmission electron micrographs of synapses from neurons high-pressure frozen in 1.2 mM Ca^{2+} either without (**e**) or with (**f**) TTX, which prevents AP firing. Samples were frozen either with no stimulation (No stim) or 5 ms after stimulation, which presumably initiates an action potential (5 ms after AP). The arrow indicates a pit in the active zone, which is presumed to be a synaptic vesicle fusing with the plasma membrane. The active zone is defined as the presynaptic plasma membrane opposite the postsynaptic density (PSD). Scale bar, 100 nm. Electron micrographs are from experiments described in Fig. 3 (from two experiments from separate cultures frozen on different days, except for the data from the TTX treatment without stimulation, which are from a single experiment, and data from 5 and 8 ms, which are from three experiments). See Supplementary Table 1 for full pairwise comparisons and summary statistics.

and discharged with a flash of light to generate a 1-ms 10 V cm^{-1} stimulus before freezing at defined time points (Methods).

To test whether this device is functional, we performed FM 1-43 dye-loading experiments in mouse hippocampal neurons cultured on 6-mm sapphire disks. The lipophilic FM dye is taken up by compensatory endocytosis after synaptic vesicle fusion[15]. To prevent destaining by exocytosis, we applied Pitstop 2 (30 μM) 2 min before loading. Pitstop 2 is a nonspecific[16] but nonetheless potent inhibitor of clathrin-mediated vesicle formation[17]. The dye is taken up during clathrin-independent ultrafast endocytosis but will be trapped in synaptic endosomes, which are resolved by clathrin-mediated budding[18]. Neurons were stimulated 10 times at 20 Hz, each pulse lasting 1 ms, which induces a single action potential. Following stimulation and fixation, presynaptic terminals were strongly labeled with FM

1-43 (threefold increase relative to no-stimulus control, $P=0.003$; Fig. 1b,c and see Extended Data Fig. 2c for full fields of view from micrographs), which suggests that the stimulation device triggers action potentials and synaptic activity.

With the stimulation device validated, we next tested whether exocytic intermediates can be captured by high-pressure freezing. Experiments were performed at 37 °C and with 1.2 mM external calcium, which is roughly the [Ca^{2+}] of the interstitial fluid in the brain[19]. We applied a single 1-ms pulse, which likely triggers a single action potential[20]. Cells were frozen 5 ms after stimulation (Fig. 1d–f), which is the earliest possible time point given the mechanics of the high-pressure freezer (Methods). At 5 ms, we may miss many fusion events that have already collapsed into the plasma membrane. However, previous reports indicate that full collapse of all vesicles takes at least several milliseconds[1,7]. Thus, we reasoned that 5 ms may be early enough to capture fusion. Samples were then prepared for electron microscopy, and images were acquired and quantified in a blinded manner (Methods). We defined the active zone as the membrane domain directly apposed to the postsynaptic density (Fig. 1e,f). We quantified any active zone membrane deflections greater than 10 nm by visual inspection as fusion pits. Although vesicle membranes may translocate by a few nanometers as they collapse, we consider the locations of pits as the sites of fusion since it has been previously reported that pits are only visible at release sites and are not accompanied by visible deflections throughout the plasma membrane[1,7]. If similar deflections are found outside the active zone, they are measured but considered endocytic[7] or membrane ruffles and thereby not included in the data (see Extended Data Fig. 2a,b for examples of features quantified as pits or not). We also counted the number of vesicles that were 0–100 nm above the plasma membrane within the area of the active zone and classified those that appeared to be in physical contact with the plasma membrane as docked (0 nm from the plasma membrane). In stimulated samples, 18% of the synaptic profiles exhibited exocytic pits in the active zone (57 out of 316), whereas in unstimulated cells, only 2% of the synaptic profiles exhibited pits (6 out of 275). Moreover, in cells in which action potentials were blocked by tetrodotoxin (TTX), only 1% of the profiles contained pits (2 out of 256; Fig. 1f). Thus, the device induces bona fide action potentials and vesicle fusion that can be reliably captured in electron micrographs. In an analogy to the previously developed flash-and-freeze method[8], this technique is called zap-and-freeze.

Multivesicular release is prominent in cultured hippocampal neurons. It has long been debated whether univesicular or multivesicular release predominates[21]. From single synaptic profiles, 2%

Fig. 2 | Multiple fusion events at single active zones after a single action potential. a, Frequency distributions of the number of fusion events 5 ms after an action potential (green) or without stimulation (gray) in solutions of 1.2, 2 or 4 mM Ca^{2+} (1.2 mM, no stim, $n=62$; 1.2 mM, stim, $n=68$; 2 mM, no stim, $n=64$; 2 mM, stim, $n=66$; 4 mM, no stim, $n=65$; 4 mM, stim, $n=64$ reconstructed active zones). Insets show the proportions, among the active zones that contained at least one fusion event, of zones that contained one fusion event (univesicular release (UVR)) or more than one fusion event (multivesicular release (MVR)). Fusion events are defined as 'pits' in the active zone. Including all active zones from stimulated samples, the number of pits was not significantly different in different Ca^{2+} concentrations ($P=0.88$); including only synapses with at least 1 fusion event, the number of pits was significantly greater at 4 mM than at 1.2 mM ($P=0.042$). The proportion of synapses that contained at least 1 pit was not different between samples stimulated in different Ca^{2+} concentrations ($\chi^2=0.2771$, d.f. = 2, $P=0.87$). **b**, Cumulative relative frequency distributions of locations of docked vesicles (with and without stimulation) and pits (after stimulation) within the active zone (*n* = 34, 54 and 70 pits; 384, 768 and 778 docked vesicles without stimulation; 384, 579 and 423 docked vesicles with stimulation, ordered by increasing Ca^{2+} concentration). Locations are normalized to the size of the active zone and to the expected density of objects within a circular area by taking the square of the distance of a pit or vesicle to the center of the active zone divided by the half-length of the active zone. On this basis, 0.25 would indicate a vesicle or pit halfway between the center and the edge. Docked vesicles were not biased toward the center or edge except for samples frozen in 4 mM Ca^{2+}, which were biased toward the center, and samples frozen after stimulation in 2 mM Ca^{2+}, which were biased toward the edge (1.2 mM, no stim, $P=0.26$; 1.2 mM, stim, $P=0.14$; 2 mM, no stim, $P=0.142$; 2 mM, no stim, 2 mM Ca^{2+}, stim, $P=0.02$; 4 mM Ca^{2+}, no stim, $P<0.001$; 4 mM Ca^{2+}, stim, $P<0.001$). Vesicle fusions were not biased toward the center or the edge ($P>0.9$ for 1.2 mM and 2 mM, $P=0.05$ for 4 mM). For each calcium concentration, the median location of pits and docked vesicles in the active zone after stimulation were similar to those of docked vesicles from no-stimulus controls ($P>0.9$ for each). **c**, The number of docked vesicles in each active-zone reconstruction 5 ms after an action potential (green) or without stimulation (gray); same *n* values as in **a**. The number of docked vesicles was not significantly different between synapses with pits (w pits) and without pits (w/o pits) for each calcium concentration ($P>0.1$ for each comparison; Kruskal–Wallis test with post hoc Dunn's multiple comparisons). Vesicles that appeared to be in contact with the plasma membrane were considered docked. Error bars indicate the median and interquartile range. **d**, Quantification of widths at the base of pits in the active zone. Error bars indicate the median and interquartile range. $n=34$, 54 and 70 pits, ordered by increasing Ca^{2+} concentration. **e**, The cumulative relative frequency distributions of distances from the center to center of pits within the same active zone, sorted by external calcium concentration. The inset shows the same data, but as dot plots. Although the median distance increases with increasing calcium, the most tightly coupled pits are still present. Error bars indicate the median and interquartile range. **f**, The cumulative relative frequency distributions of distances from center to center of pits and docked vesicles within the same active zone ($n=218$ pairs of pits, 5,438 pairs of docked vesicles; see Methods for a description of distance calculation). Pit-to-pit distances were slightly greater than docked vesicle-to-docked vesicle distances (pits median: 224 nm; docked median: 265 nm; $P=0.02$). Pairs of pits were from stimulated samples in 4 mM Ca^{2+}; pairs of docked vesicles were from the no-stimulus 4 mM Ca^{2+} experiment. SV, synaptic vesicle. All data are from two experiments from separate cultures frozen on different days; experiments in 1.2 mM Ca^{2+} were performed on separate days from a separate culture from the experiments in 2 mM and 4 mM Ca^{2+}. The number of pits and docked vesicles per active zone (**a** and **b**) was compared using Kruskal–Wallis tests with post hoc Dunn's multiple comparisons test. For pits, full pairwise comparisons were performed; for docked vesicles, only the numbers of vesicles before and after stimulation at each Ca^{2+} concentration were compared. The proportions of active-zone reconstructions that contained at least one pit were compared using a chi-square test. The bias of pit locations toward the center or edge of the active zone was tested by comparing each group to a theoretical median of 0.5, the expected median for a random distribution, using two-tailed one-sample Wilcoxon signed-rank tests. The locations of pits, docked vesicles after stimulation and docked vesicles without stimulation were compared using a Kruskal–Wallis test followed by post hoc Dunn's test between pits and no-stimulus docked vesicles and stimulated docked vesicles and no-stimulus docked vesicles for each calcium concentration. *P* values from all these pairwise and one-sample comparisons were adjusted with Bonferroni correction accounting for the total number of tests. The distances between pits in different calcium concentrations were compared using a Kruskal–Wallis test followed by post hoc Dunn's test. The distributions of distances between pits in the same active zone and docked vesicles within the same active zone were compared using a two-sided Wilcoxon rank-sum test. See Supplementary Table 1 for full pairwise comparisons and summary statistics. See Supplementary Table 2 for summary statistics of docked vesicle and pit counts for each experimental replicate.

(6 out of 316 synaptic profiles) exhibited multiple pits. Although rare, the presence of multiple pits in the same image indicates that more than one vesicle in an active zone can fuse after a single action potential, an event known as multivesicular release[21]. However, the frequency of such events cannot be determined from single sections but requires the reconstruction of entire active zones from serial sections (Fig. 2). To quantify synaptic vesicle fusions per synapse, cultured hippocampal neurons were stimulated in 1.2 mM Ca^{2+} at 37 °C and frozen 5 ms after stimulation. Over 60 active zones were reconstructed for each condition, and morphometry was performed in a blinded manner (see Extended Data Fig. 3a for example micrographs). In unstimulated samples, 3% of the synapses contained a pit (2 out of 62), whereas in stimulated samples, 35% of the synapses exhibited at least one pit (24 out of 68; Fig. 2a). Of those with at least 1 pit, 38% of active zones (9 out of 24) contained multiple pits. All pits ranged from the size of a synaptic vesicle to expected sizes of vesicles at late stages of collapse into the plasma membrane (the full range of pit widths at the base was 24–89 nm; Fig. 2d). These results suggest that multivesicular release is prominent in cultured hippocampal neurons.

Multivesicular release is augmented by increasing extracellular calcium. To further assess the number of release sites per active zone, we enhanced the release probability by increasing the extracellular calcium concentration from 1.2 mM to 2 mM and 4 mM calcium. Fusion was assessed by the presence of pits in the reconstructed active zones. Increasing the extracellular Ca^{2+} concentration did not change the fraction of synapses with visible fusions (Fig. 2a). That is, at all calcium concentrations, only ~35% of active zones exhibited fusion pits (pits per active zone: 1.2 mM: 35%

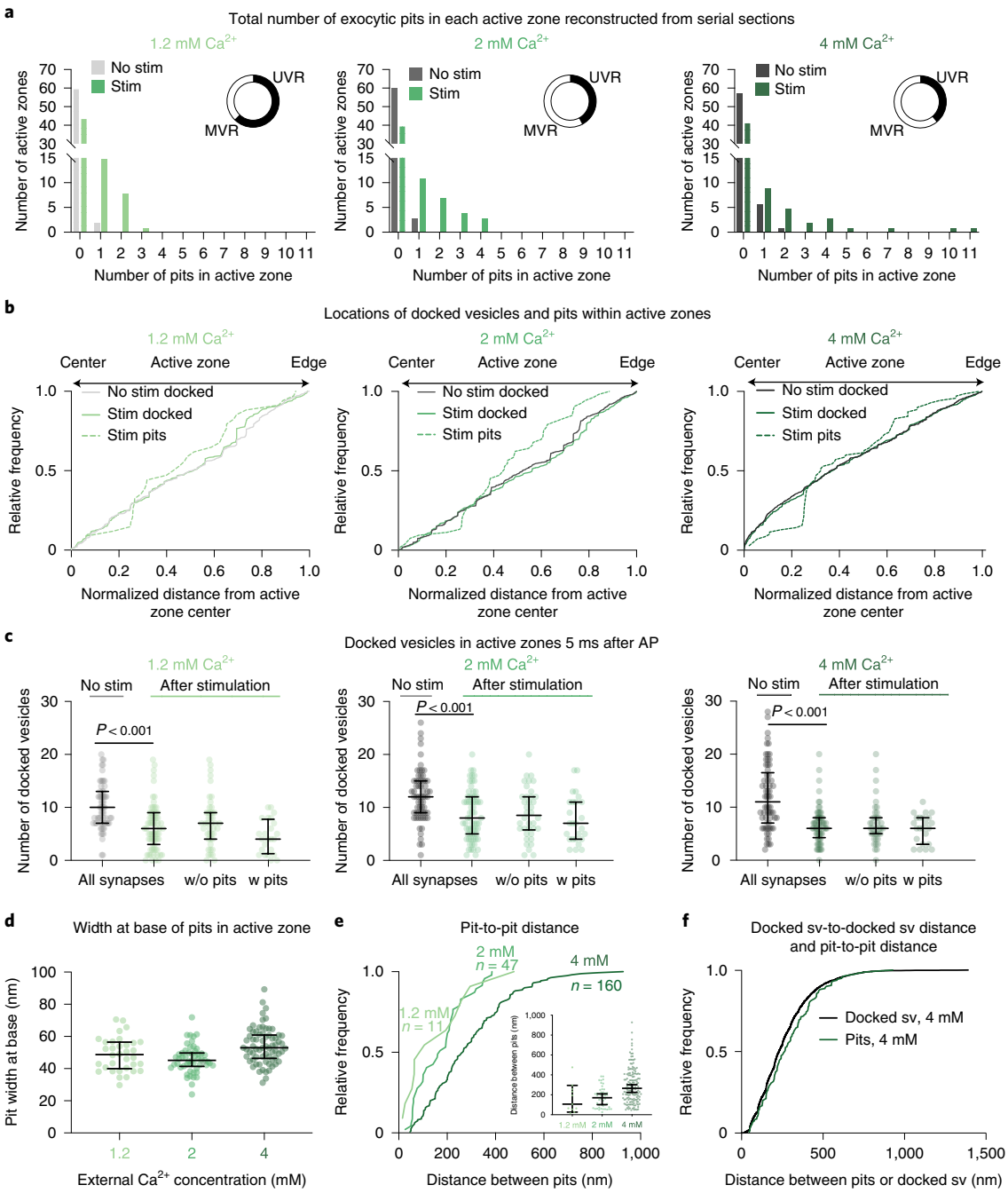

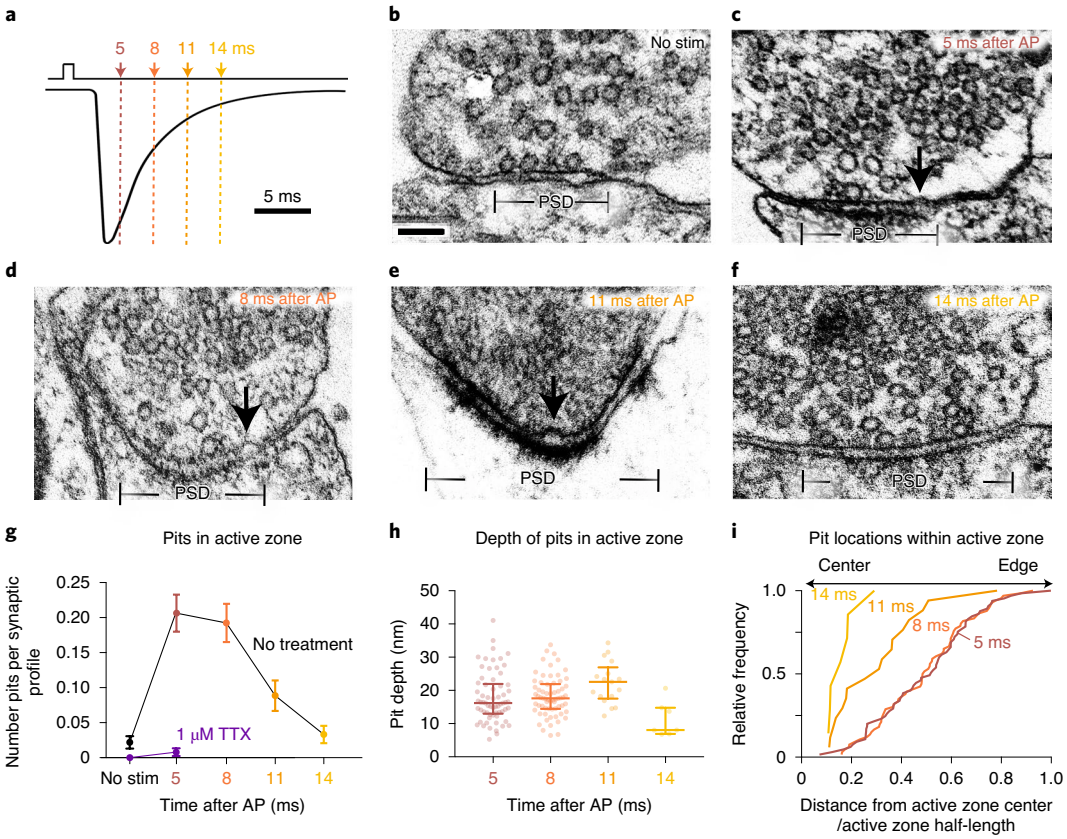

Fig. 3 | Vesicle fusion during the first 14 ms after an action potential. a, Experimental design for stimulation and freezing, showing a diagrammatic excitatory postsynaptic current for reference (based on ref. [28]). A 1-ms square pulse is applied to trigger a single action potential, then neurons are frozen at the indicated time points after the beginning of the pulse. **b**–**f**, Example transmission electron micrographs of synapses from neurons frozen without stimulation (**b**) and 5 ms (**c**), 8 ms (**d**), 11 ms (**e**) or 14 ms (**f**) after stimulation. Arrows indicate pits in the active zone, which are presumed to be synaptic vesicles fusing with the plasma membrane. Scale bar, 100 nm. **g**, The number of pits in the active zone per synaptic profile (part of the synapse captured in a 2D section) in the above conditions, and without stimulation or 5 ms after stimulation in TTX (1 μM, purple). No stim, $n = 274$; 5 ms, $n = 315$; 8 ms, $n = 343$; 11 ms, $n = 192$; 14 ms, $n = 211$; TTX, no stim, $n = 121$; and TTX, 5 ms, $n = 255$ synaptic profiles. The numbers of pits with and without stimulation in TTX were not significantly different ($P > 0.9$). The numbers of pits at 14 ms and without stimulation were not significantly different ($P > 0.9$). **h**, The depth of pits within the active zone 5 ms ($n = 65$ pits), 8 ms ($n = 66$ pits), 11 ms ($n = 17$ pits) and 14 ms ($n = 7$ pits) after stimulation. The depth of pits at different time points were all similar (5 ms versus 8 ms, $P > 0.9$; 5 ms versus 11 ms, $P = 0.05$; 5 ms versus 14 ms, $P = 0.14$; 8 versus 11 ms, $P = 0.22$; 8 versus 14 ms, $P = 0.05$), except for 11 ms and 14 ms, which were significantly different from each other ($P = 0.002$). **i**, Locations within the active zone of the same pits described in **h**. The pits at 11 ms were biased toward the center of the active zone ($P = 0.004$), while those at 5 ms and 8 ms were not biased toward the center or the edge ($P > 0.9$ in both cases). Error bars in **g** indicate the s.e.m.; error bars in **h** and **i** indicate the median and interquartile range. All data are from two experiments from separate cultures frozen on different days, except for the data from TTX treatment without stimulation, which are from a single experiment, and data from 5 and 8 ms, which are from three experiments. The numbers of pits in **g**, the locations of pits in **h** and the heights of pits in **i** were compared using Kruskal–Wallis tests with full pairwise comparisons by post hoc Dunn's multiple comparisons tests. The bias of pit locations toward the center or edge of the active zone was tested by comparing each group to a theoretical median of 0.5 using one-sample two-tailed Wilcoxon signed-rank tests; Bonferroni correction was applied to all P values from multiple-sample and one-sample tests to account for these extra comparisons. See Supplementary Table 1 for full pairwise comparisons and summary statistics. See Supplementary Table 2 for summary statistics of pit counts for each experimental replicate.

(24 out of 68); 2 mM: 39% (26 out of 66); 4 mM: 34% (23 out of 64); $P = 0.87$). However, increasing the calcium concentration did augment multivesicular release. At 1.2 mM Ca^{2+}, 38% of active zones containing at least 1 fusion exhibited multivesicular release, whereas at 2 mM Ca^{2+}, 58% exhibited multivesicular release. At 4 mM Ca^{2+}, 61% exhibited multivesicular release, including 1 active zone with 11 pits (Extended Data Fig. 3). Thus, multivesicular release is present at physiological calcium concentrations, and at elevated calcium concentrations, is responsible for the vast majority of vesicle fusion.

Release events can be coupled. The presence of several pits within single active zones suggests that each synapse likely has more than one release site. This is consistent with the localization pattern of many proteins that are essential for neurotransmitter release, including calcium channels. These proteins are clustered, and several clusters seem to be distributed throughout the active zone[22–24]. To assess the distribution of release sites within active zones at the ultrastructural level, we mapped the locations of docked vesicles and exocytic pits (Extended Data Fig. 4a,b). At low calcium concentrations, fusing vesicles were often found adjacent to each other (Extended Data Figs. 2 and 3), which suggests that neighboring vesicles fuse simultaneously (Fig. 2e). At 1.2 mM Ca^{2+}, pits were often within ~100 nm of each other (median of 106 nm, $n = 11$ pairs). With increasing calcium concentrations, adjacent fusions were still observed, but additional pits were dispersed across the active zone (2 mM Ca^{2+}: median of 171 nm, $n = 47$ pairs; 4 mM Ca^{2+}: median of

265 nm, $n = 160$ pairs; Fig. 2e). At 4 mM Ca^{2+}, the median distance between pits was roughly similar to the distance between docked vesicles (docked = 229 nm; pits = 265 nm; $P = 0.02$; Fig. 2f). Thus, at high calcium concentrations, release sites act independently; that is, there is neither an obvious coupling of release sites across an active zone nor evidence of lateral inhibition[25]. By contrast, at low calcium concentrations, adjacent vesicles tend to fuse together, possibly via a common calcium microdomain.

Docking is not a stable state. Docked vesicles are often referred to as release-ready vesicles[4]. Indeed, numbers of docked vesicles were profoundly decreased after stimulation (Fig. 2c, 'all synapses'). However, the degree of docked vesicle depletion was much more severe than expected from the number of pits we observed. At 1.2 mM Ca^{2+}, the median number of docked vesicles decreased from ten to six following stimulation for all synapses ($P < 0.001$; see Extended Data Fig. 4c,d for the number of docked vesicles and pits per 10,000 nm^2 of active zone membrane). Therefore, an average of about four pits should be observed in every active zone, but only 35% of synapses contained exocytic pits. To match the loss of docked vesicles, among these 35% there would need to be an average of about ten vesicles fusions per active zone. However, in the active zones that contained pits, the median number of pits was just one. Likewise, at 2 mM Ca^{2+}, docked vesicles decreased from 12 to 8 at 2 mM ($P < 0.001$), and the median number of pits was 2 per pit-containing active zone. At 4 mM Ca^{2+}, docked vesicles decreased from 11 to 6 ($P < 0.001$), and the median number of pits was 2 per pit-containing active zone. Increasing the external calcium concentration did not augment the percentage of active zones that respond to an action potential (~35%). Thus, we either missed a massive number of fusions (>80% to account for the loss of docked vesicles) or observed activity-dependent undocking of synaptic vesicles[14].

Interestingly, synapses that did not have pits also exhibited a profound and roughly equal depletion of docked vesicles (Fig. 2c, 'w/o pits' versus 'w pits'). One could imagine that non-responding synapses were just smaller and initially had fewer docked vesicles[26]. However, the active zone size was comparable between those with and without pits (Extended Data Fig. 4e). The absence of pits in these synapses suggests that these synapses are inactive, and that the loss of docking at these synapses is not just the result of fusions that we failed to detect. These data imply that docking is not a stable state and that vesicles can stay docked, fuse or potentially undock after stimulation.

Fusing vesicles at 11 ms represent asynchronous release. To determine whether vesicles continue to fuse after the 5-ms time point and how these release sites are reoccupied on a short time scale, we performed morphometry on synaptic profiles frozen at 5, 8, 11 and 14 ms after an action potential (1.2 mM Ca^{2+}, 37 °C; Fig. 3a–f and Extended Data Fig. 5a,b). Pits peaked at 5 and 8 ms, then declined to baseline by 14 ms (pits per profile: no stimulus: 0.02; 5 ms: 0.21; 8 ms: 0.19; 11 ms: 0.09; 14 ms: 0.03) (Fig. 3g and see Extended Data Fig. 5f for sizes of active zone sizes and Extended Data Fig. 5g for the number of pits per 100 nm of active zone). The depth of pits at 5 ms was variable (median of 16.2 nm, interquartile range of 13.2–22.7 nm; Fig. 3h), which suggests that some pits had collapsed by this time. Unexpectedly, pits at 11 ms were slightly deeper than those at 5 ms (median at 5 ms: 16.2 nm; at 11 ms: 21.7 nm; $P = 0.05$; Fig. 3h). The presence of deep pits suggests that fusion of these vesicles may have initiated later, and may therefore represent asynchronous release[27].

To specifically test for asynchronous fusion, we assayed exocytosis in the presence of the slow calcium chelator EGTA-AM (25 µM). Intracellular EGTA-AM has a minor effect on synchronous release at most synapses[28] because the delay between calcium influx and vesicle fusion is less than a millisecond[29]. By contrast, it abolishes slower, asynchronous release[30]. In controls treated with dimethylsulfoxide (DMSO), pits were apparent in active zone profiles at 5 and 11 ms (pits per synaptic profile: at 5 ms: 0.16 pits; at 11 ms: 0.14 pits) (Fig. 4a and see Extended Data Fig. 6a for more micrographs, Extended Data Fig. 5c for active zone sizes and Extended Data Fig. 5e for the number of pits per 100 nm of active zone). Treatment with EGTA-AM (25 µM) had no effect at 5 ms, but eliminated fusion events at 11 ms (pits per synaptic profile: 5 ms: 0.18 pits; 11 ms: 0.04 pits; $P < 0.001$) (Fig. 4b,c and see Extended Data Fig. 6b for more micrographs). Thus, the collapse of newly fused vesicles must be rapid (less than 11 ms), and the speed of collapse is therefore faster than our previously calculated time constant of 20 ms[7]. These data demonstrate that fusion events observed at 5 and 11 ms represent synchronous and asynchronous release, respectively.

Asynchronous fusion is concentrated at the center of the active zone. Vesicle fusions occurring during synchronous release were found throughout the active zone, with a slight depletion at the center, in three-dimensional (3D) reconstructions of synapses (Fig. 2b). Docked vesicles were generally found throughout the active zone without bias toward the center or edge (Fig. 2b and see Supplementary Table 1 for details). Following stimulation, the distribution of docked vesicles within the active zone was unchanged ($P > 0.1$ for each; Fig. 2b). However, pits were slightly less abundant at the center at all calcium concentrations (Fig. 2b), which suggests that vesicles at the center are initially less fusion-competent.

In single profiles, a lack of bias was also observed during synchronous release. Indeed, pits and docked vesicles at 5 and 8 ms were not biased toward the center or edge of the active zone (5 ms and 8 ms, $P > 0.4$ in all cases; Figs. 3i and 4d and Extended Data Fig. 5c). By contrast, pits at 11 and 14 ms were found near the center of the active zone more frequently, and these distributions were significantly different from those at 5 and 8 ms ($P = 0.004$ (Fig. 3i) $P < 0.001$ (Fig. 4d)). Together, these data argue that vesicles fuse throughout the active zone during synchronous release, whereas asynchronous release is concentrated near the center of the active zone.

Vesicles transiently dock after synchronous release. As synaptic vesicles are consumed during synchronous and asynchronous release, new vesicles must be recruited to the active zone. During synchronous fusion, docked vesicles across all synaptic profiles were reduced by ~40% (docked vesicles per profile: no stimulus: 1.6 vesicles; 5 ms: 0.9 vesicles; 8 ms: 1.0 vesicles; $P < 0.001$) (Fig. 5a,b and see Fig. 2c for 3D analysis at 5 ms and see Extended Data Fig. 5h for the number of docked vesicles per 100 nm of active zone). During this time, the number of vesicles close to the membrane but not docked (between 6 and 10 nm) slightly increased (Fig. 5c and Extended Data Fig. 6d), which possibly reflects vesicles undocked from the active zone (Fig. 2c) or recruited from the cytoplasm. During asynchronous fusion, docked vesicles were not further depleted despite ongoing fusion, which implies that synaptic vesicles are recruited during this process (11- ms time point: 1.0 docked vesicles per synaptic profile; $P > 0.9$ versus 5 ms and 8 ms; $P < 0.001$ versus no stimulus; Fig. 5a). Strikingly, at 14 ms, docked vesicles were fully restored to pre-stimulus levels (1.4 docked vesicles per profile, $P > 0.9$ versus no stimulus; Fig. 5a).

The replacement of many forms of release-ready vesicles is known to depend on calcium[12,31,32]. We tested whether this ultrafast docking was sensitive to intracellular calcium chelation. Cells were treated with EGTA-AM for 30 min, stimulated and then frozen. EGTA-AM treatment had no effect on the number of docked vesicles in unstimulated samples or on the number of vesicles docked at 5 or 11 ms compared to the control (docked vesicles per synaptic profile: no-stimulus control: 2.0; 5-ms time point: 1.2; 11-ms time point: 1.1; $P > 0.2$ versus DMSO control for each) (Fig. 5b and see Extended Data Fig. 6f for the number of docked vesicles per 100 nm

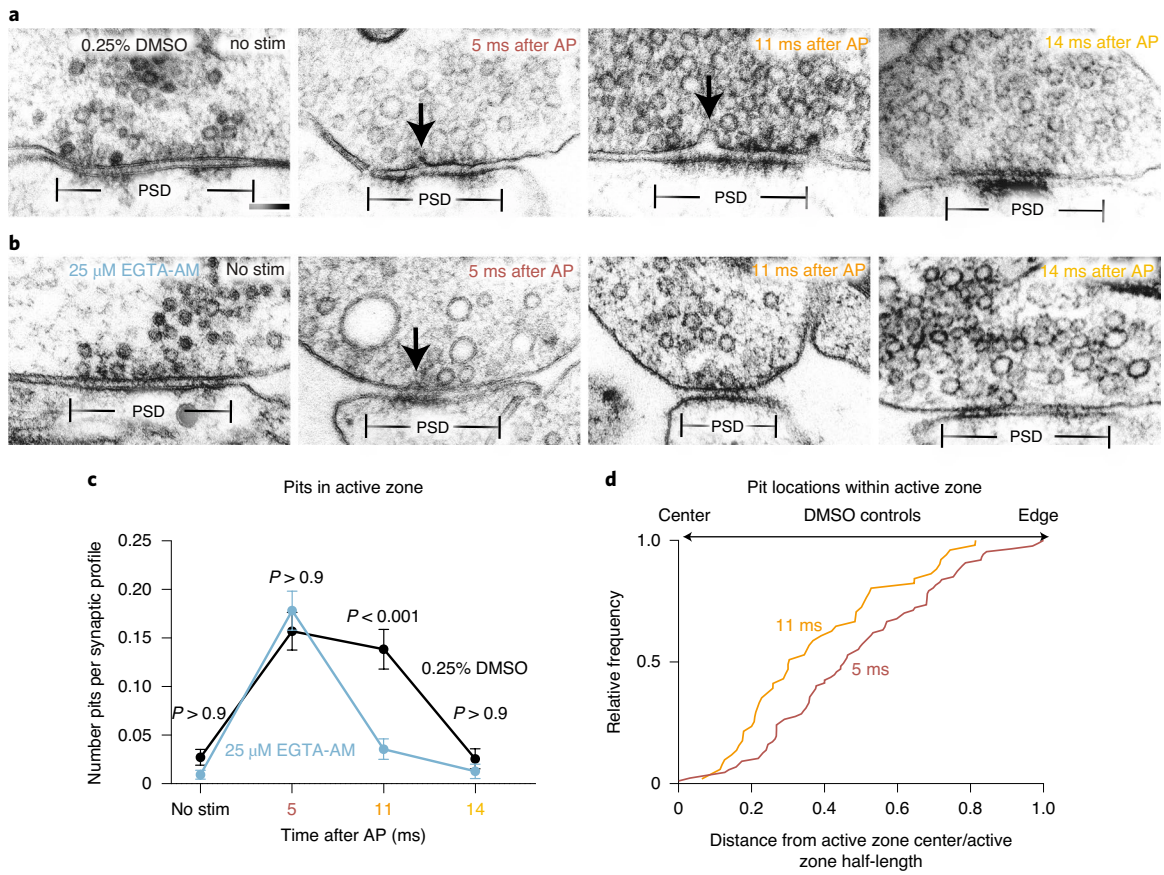

Fig. 4 | Fusions captured at 5 and 11 ms after an action potential represent synchronous and asynchronous release. a,**b**, Example transmission electron micrographs of synapses from neurons pretreated with 0.25% DMSO (**a**) or 25 μM EGTA-AM (**b**) and frozen either without stimulation, 5 ms after stimulation, 11 ms after stimulation or 14 ms after stimulation. Arrows indicate pits in the active zone, which are presumed to be synaptic vesicles fusing with the plasma membrane. Scale bar, 100 nm. **c**, The number of pits in the active zone per synaptic profile (part of the synapse captured in a 2D section) in the above conditions. *P* values are from comparisons between EGTA-treated (no stim, $n=430$; 5 ms, $n=421$; 11 ms, $n=365$; 14 ms, $n=236$ synaptic profiles) and DMSO-treated (no stim, $n=405$; 5 ms, $n=465$; 11 ms, $n=318$; 14 ms, $n=235$ synaptic profiles) samples frozen at the same time point. The numbers of pits at 11 ms and without stimulation in EGTA-AM-treated samples were not significantly different ($P>0.9$). **d**, Locations of pits within the active zone 5 ms ($n=87$ pits) and 11 ms ($n=51$ pits) after stimulation from neurons pretreated with 0.25% DMSO. Pits at 11 ms were significantly biased toward the center of the active zone ($P<0.001$), while those at 5 ms were not biased toward the center or the edge ($P>0.9$). Error bars in **c** indicate the s.e.m. All data from the experiments are from 4 experiments for no stimulus and 5-ms time points, 3 experiments for 11 ms and 2 experiments for 14 ms from separate cultures frozen on different days (see Supplementary Table 2 for count data from each experiment). The numbers of pits in **c** were compared using a Kruskal–Wallis test with full pairwise comparisons by post hoc Dunn's multiple comparisons test (only comparisons between the same time point with and without EGTA-AM are shown). Locations of pits in **d** were compared using a two-sided Wilcoxon rank-sum test. The bias of pit locations toward the center or edge of the active zone was tested by comparing each group to a theoretical median of 0.5 using one-sample two-tailed Wilcoxon signed-rank tests; Bonferroni correction was applied to all *P* values from two-sample and one-sample tests to account for these extra comparisons. See Supplementary Table 1 for full pairwise comparisons summary statistics. See Supplementary Table 2 for summary statistics of pit counts for each experimental replicate.

of active zone). However, at 14 ms, docked vesicles no longer recovered to baseline (14-ms time point: 1.1 docked vesicles per synaptic profile; $P>0.9$ versus 5 and 11 ms; $P<0.001$ versus no stimulus; $P<0.001$ versus DMSO 14 ms) (Fig. 5b). These data indicate that the fast recovery of docked vesicles occurring during vesicle fusion is calcium-dependent.

We have previously observed that docked vesicle replenishment is slow, whereby docked vesicles are depleted by 50 ms and returned to baseline by 10 s with a time constant of 3.8 s[7]. Similarly, using zap-and-freeze, docked vesicles were reduced by 30% at ~100 ms (docked vesicles per synaptic profile: no stimulus: 1.8 ; 105 ms: 1.2; $P<0.001$) (Fig. 5d). Docked vesicle levels were still 25% lower than unstimulated samples at 1 s after stimulation, but docking was fully recovered by 10 s (docked vesicles per synaptic profile: no stimulus: 1.71; 100 ms: 1.0; 1 s: 1.37; 10 s: 1.66; $P<0.001$ between no stimulus and 105 ms; $P=0.002$ between no stimulus and 1 s; $P>0.9$ between no stimulus and 10 s) (Fig. 5e). Therefore, the fast, calcium-dependent replenishment of docked vesicles observed at 14 ms is temporary and appears to be lost within 100 ms, and transient docking is followed by a slower docking process that requires 3–10 s. Transient docking[9] could provide fusion-competent vesicles for asynchronous release[13] and counteract synaptic depression during trains of stimuli[9].

Discussion

We characterized the docking and exocytosis of synaptic vesicles at hippocampal synapses in ultrastructural detail. The findings reported here have implications for multivesicular release, the spatial organization of release sites and their refilling during short-term plasticity.

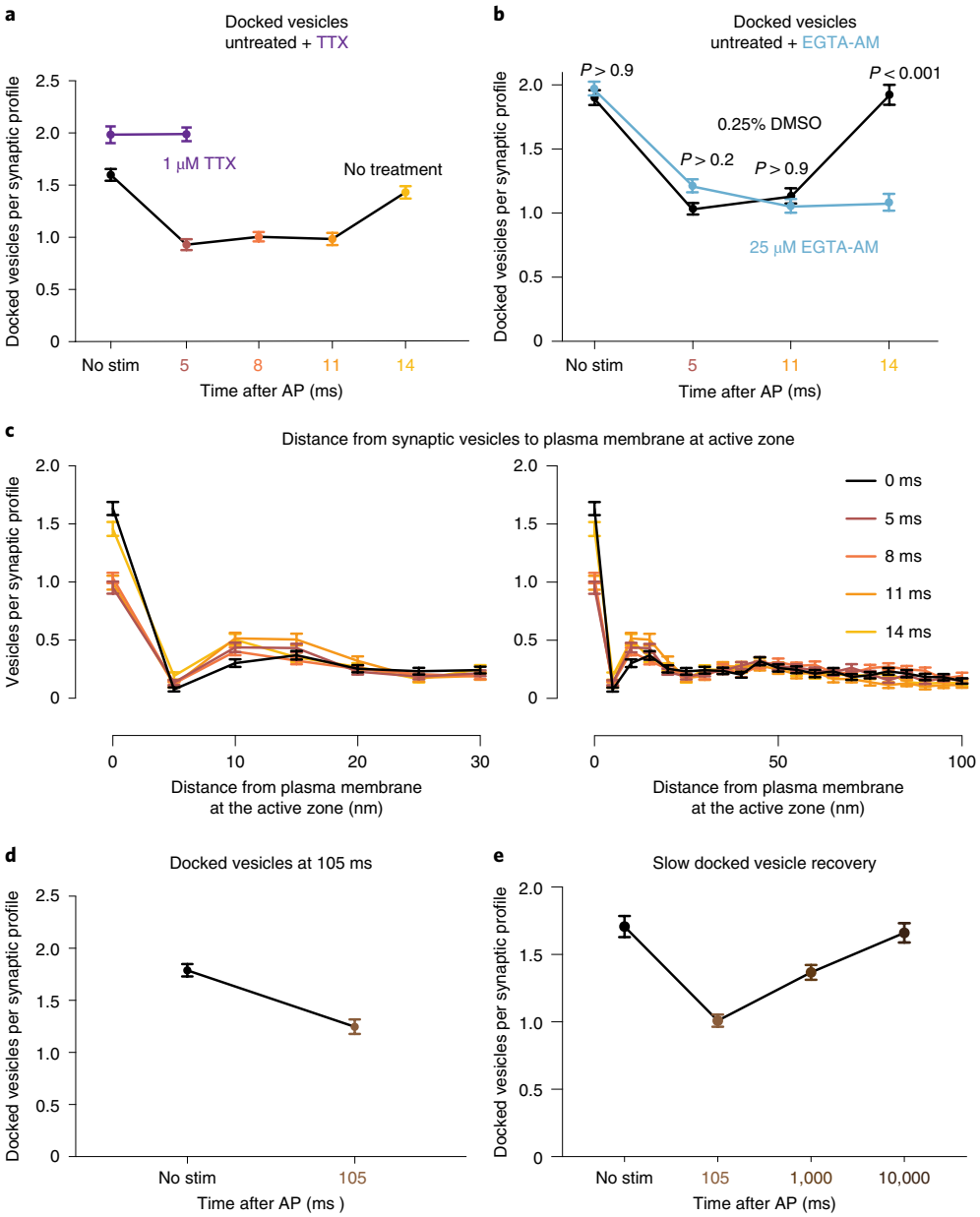

Fig. 5 | Transient docking refills the docked vesicle pool within milliseconds. a, The number of docked vesicles per synaptic profile (part of the synapse captured in a 2D section) from the same experiments and synaptic profiles as in Fig. 3. The number of docked vesicles at 14 ms was not significantly different from the no-stimulation control ($P > 0.9$). **b**, Same as **a**, except from the experiments in Fig. 4. The number of docked vesicles at 14 ms in the DMSO control was not significantly different from the no-stimulation control ($P > 0.9$), but was significantly different from results of the EGTA-AM treatment ($P < 0.001$). **c**, Distances of synaptic vesicles from the plasma membrane at the active zone, including vesicles that were annotated as docked and as not docked (left panel is a zoom-in of the 6–10-nm bin). Distances are binned in 5-nm increments, except for "0", which indicates vesicles ~0 nm from the active zone membrane ("5" indicates vesicles 0.1–5 nm from the membrane, "10" indicates 6–10 nm, and so on). The number of vesicles at 0 (docked) was significantly greater in the no-stimulus control than at all other time points but 14 ms (see *P* values listed for **a**). The only other multiplicity-corrected *P* values less than 0.05 at any distance were for 11 ms ($P = 0.014$) and 14 ms ($P = 0.048$) at 6–10 nm (shown in zoomed panel on the left). **d**, The number of docked vesicles without stimulation or 105 ms after an action potential (no stim, $n = 209$; 105 ms, $n = 218$ synaptic profiles). **e**, The number of docked vesicles without stimulation or 105 ms, 1 s or 10 s after an action potential with 4 mM extracellular [Ca^{2+}] (no stim, $n = 205$; 105 ms, $n = 328$; 1 s, $n = 313$; 10 s, $n = 212$). Vesicles that appeared to be in contact with the plasma membrane were considered docked. The numbers of docked vesicles in **a** and **b** were compared using a Kruskal–Wallis test with full pairwise comparisons by post hoc Dunn's multiple comparisons test. The distances of synaptic vesicles from the active zone in the first five bins of data shown in **c** (0–25 nm from the active zone) were compared to the no-stimulus control using a one-way ANOVA with post hoc Games–Howell's test, with all pairwise comparisons further multiplicity-corrected using the Bonferroni method to account for the five ANOVA tests. The number of docked vesicles in **d** were compared using a two-sided Wilcoxon rank-sum test. The number of docked vesicles in **e** were compared using a Kruskal–Wallis test with post hoc Dunn's test. Error bars represent the s.e.m. See Supplementary Table 1 for full pairwise comparisons and summary statistics. See Supplementary Table 2 for summary statistics for each experimental replicate.

The presence of multiple vesicles docked at a synapse alone does not imply that multiple vesicles can fuse at an active zone. In fact, it was long thought that only one vesicle could fuse in response to an action potential[21,33]. These studies argued that responses at synapses are mostly, or even exclusively, uniquantal. For proponents of univesicular release, examples of recordings of multivesicular events were dismissed as being caused by multiple active zones impinging on the cell. Proponents of multiquantal release at single active zones argued that observations of uniquantal events were due to saturation of the postsynaptic receptor field, and multiquantal release could be observed under circumstances in which saturation could be avoided[34–36]. By reconstructing synapses from serial sections immediately after a single action potential, we were able to capture multiple vesicles fusing in a single active zone. At 4 mM calcium, we observed up to 11 vesicles fusing in a single active zone. The probability of fusion at a release site appears to be low even at elevated calcium levels, but because active zones have approximately ten docking sites, multiple vesicles can be consumed by a single action potential.

Importantly, fusing vesicles tended to be close (<100 nm) to one another at low calcium concentrations, and were in fact often adjacent. Adjacent fusions can also be observed during spontaneous activity: in a previous study[37], 20% of synaptic profiles exhibiting spontaneous fusions comprised adjacent fusions, which suggests that fusing vesicles are coupled even in the absence of stimulation[37]. It is likely that coupled fusion is being driven by an active calcium channel or calcium microdomain that acts on locally docked vesicles[29,38,39].

In contrast to the microdomains that drive synchronous release, the residual calcium that triggers asynchronous release is more broadly distributed and longer lasting[27,40]. This implies that there would be no spatial specificity for asynchronous fusion. However, we found that asynchronous release occurs preferentially near the center of the active zone. Several molecules, including VAMP4 (ref. [41]), synaptotagmin-7 (ref. [42]), SNAP23 (ref. [43]) and DOC2 (ref. [44]), have been implicated in asynchronous release, and these molecules could target vesicles to release sites near the center of an active zone. Alternatively, the locations of voltage-gated calcium channel clusters within an active zone may account for this spatial arrangement. In neuromuscular junctions of both *Caenorhabditis elegans*[45] and *Drosophila melanogaster*[46], different isoforms of Unc13 position vesicles at different distances from the dense projection, where calcium channels reside[47]. These clusters are proposed to form independent release sites for fast and slow phases of neurotransmission. In conclusion, while the molecular mechanism remains uncertain, synchronous and asynchronous release are concentrated in different regions of the active zone.

A profound decrease in docking was observed after stimulation. The fusions we observed can only account for ~30% of the decrease in docking. Moreover, docking is also reduced in synapses with no visible fusions. The loss of docked vesicles is accompanied by a slight increase in vesicles 6–10 nm from the plasma membrane, which suggests that these vesicles may still be tethered to the membrane by a loosely assembled SNARE complex, by synaptotagmin or by Munc13 (ref. [4]). However, it is equally possible that more vesicles are recruited to this region from the cytoplasm. Furthermore, the increase in vesicles 6–10 nm from the plasma membrane cannot fully account for the massive loss of docked vesicles, which leaves their fate uncertain. Therefore, we conclude that either ~40% of docked vesicles across all synapses fuse after a single action potential or vesicles become undocked after a single action potential, or some combination of the two.

At 14 ms after stimulation, docking levels are fully restored to pre-stimulus levels. But then by 100 ms after stimulation, docking is again reduced to the levels observed immediately after stimulation; thus, the docking that occurs 10–14 ms after the action potential is transient. We did not observe transient docking in our previous flash-and-freeze experiments[7], likely because the generation and timing of action potentials using channelrhodopsin is unreliable. However, the more prolonged reduction in docked vesicles observed here at 100 ms and 1 s is consistent with our previous results[7]. Full and stable restoration of docking was not finished until 3–10 s[7] after stimulation, which is consistent with the slow phase of recovery of the physiological readily releasable pool[11]. Thus, there is a rapid docking of vesicles after stimulation, but this docking is only transient.

What purpose could fast, but ephemeral, vesicle recruitment serve? Quite likely, it is to maintain robust synaptic transmission during trains of stimuli. Recent electrophysiological studies of a cerebellar "simple synapse" composed of a single active zone indicate that an undocked population of vesicles may occupy a "replacement site"[12,13], which possibly corresponds to our 10-nm pool. Based on modeling, vesicles in this pool are rapidly mobilized to dock at a release site. However, these docked vesicles become undocked and return to the replacement site in the 100 ms following the action potential. Transient docking is likely mediated, at least in part, by the calcium sensor synaptotagmin-1 (ref. [9]). When the membrane-binding residues of synaptotagmin-1 were mutated, vesicle docking was reduced by 30–50%. Docking was restored by an action potential, but had declined after 100 ms, which is consistent with the time course of docking that we observed. Our data demonstrate that transient docking is not just a quirk of synaptotagmin-1 mutants. Moreover, vesicles may undock before transiently redocking.

In summary, we characterized the ultrastructure of a synapse during the first 14 ms after an action potential using zap-and-freeze electron microscopy (Extended Data Fig. 1). An action potential drives the fusion of one or more vesicles, likely via a shared calcium microdomain. It is presumed that such vesicles are docked to the membrane in a "tight state" as recently proposed[14]. Stimulation is accompanied by a massive reduction of the docked pool, perhaps even in synapses that do not exhibit fusion. One possibility is that calcium drives docked vesicles into an undocked state, most likely by binding to a protein such as Munc13 or synaptotagmin-1 or possibly to a lipid such as PIP2. Alternatively, vesicles could be in a dynamic equilibrium between fusion-competent (docked) and fusion--incompetent states (undocked) at steady state near the active zone membrane, and only those that are tightly docked coincident with calcium influx would fuse. These undocked vesicles would still be associated with release sites, but are tethered ~10 nm from the membrane. Such vesicles are proposed to exist in a "loose state", with SNAREs, synaptotagmin-1 and Munc13 still engaged[48]. Between 8 and 14 ms, vesicles dock to the membrane in a calcium-dependent manner, perhaps driven by synaptotagmin-1 (ref. [9]) or the calcium sensor for facilitation synaptotagmin-7 (ref. [49]). Docking is occurring at the same time as vesicles are undergoing asynchronous fusion and may represent vesicles undergoing "two-step" release[13]. Docking levels are fully restored 14 ms after stimulation; however, this docking is not stable and declines along with falling calcium levels. This time course is similar to that of paired-pulse facilitation of synaptic transmission[50]. Thus, synaptic vesicles at the active zone exhibit surprisingly lively dynamics between docked and undocked states within milliseconds after an action potential.

Online content

Any methods, additional references, Nature Research reporting summaries, source data, extended data, supplementary information, acknowledgements, peer review information; details of author contributions and competing interests; and statements of data and code availability are available at https://doi.org/10.1038/s41593-020-00716-1.

Received: 17 April 2020; Accepted: 1 September 2020;
Published online: 28 September 2020

References

1. Heuser, J. E. et al. Synaptic vesicle exocytosis captured by quick freezing and correlated with quantal transmitter release. *J. Cell Biol.* **81**, 275–300 (1979).
2. Kaeser, P. S. & Regehr, W. G. The readily releasable pool of synaptic vesicles. *Curr. Opin. Neurobiol.* **43**, 63–70 (2017).
3. Schikorski, T. & Stevens, C. F. Quantitative ultrastructural analysis of hippocampal excitatory synapses. *J. Neurosci.* **17**, 5858–5867 (1997).
4. Imig, C. et al. The morphological and molecular nature of synaptic vesicle priming at presynaptic active zones. *Neuron* **84**, 416–431 (2014).
5. Hammarlund, M., Palfreyman, M. T., Watanabe, S., Olsen, S. & Jorgensen, E. M. Open syntaxin docks synaptic vesicles. *PLoS Biol.* **5**, 1695–1711 (2007).
6. Richmond, J. E., Weimer, R. M. & Jorgensen, E. M. An open form of syntaxin bypasses the requirement for UNC-13 in vesicle priming. *Nature* **412**, 338–341 (2001).
7. Watanabe, S. et al. Ultrafast endocytosis at mouse hippocampal synapses. *Nature* **504**, 242–247 (2013).
8. Watanabe, S. et al. Ultrafast endocytosis at *Caenorhabditis elegans* neuromuscular junctions. *eLife* **2013**, e00723 (2013).
9. Chang, S., Trimbuch, T. & Rosenmund, C. Synaptotagmin-1 drives synchronous Ca^{2+}-triggered fusion by C2B-domain-mediated synaptic-vesicle-membrane attachment. *Nat. Neurosci.* **21**, 33–42 (2018).
10. Ritzau-jost, A. et al. Ultrafast action potentials mediate kilohertz signaling at a central synapse. *Neuron* **84**, 152–163 (2014).
11. Pyott, S. J. & Rosenmund, C. The effects of temperature on vesicular supply and release in autaptic cultures of rat and mouse hippocampal neurons. *J. Physiol.* **539**, 523–535 (2002).
12. Miki, T. et al. Actin- and myosin-dependent vesicle loading of presynaptic docking sites prior to exocytosis. *Neuron* **91**, 808–823 (2016).
13. Miki, T., Nakamura, Y., Malagon, G., Neher, E. & Marty, A. Two-component latency distributions indicate two-step vesicular release at simple glutamatergic synapses. *Nat. Commun.* **9**, 3943 (2018).
14. Neher, E. & Brose, N. Dynamically primed synaptic vesicle states: key to understand synaptic short-term plasticity. *Neuron* **100**, 1283–1291 (2018).
15. Betz, W. J. & Bewick, G. S. Optical analysis of synaptic vesicle recycling at the frog neuromuscular junction. *Science* **255**, 200–203 (1992).
16. Dutta, D., Williamson, C. D., Cole, N. B. & Donaldson, J. G. Pitstop 2 is a potent inhibitor of clathrin-independent endocytosis. *PLoS ONE* **7**, e45799 (2012).
17. Von Kleist, L. et al. Role of the clathrin terminal domain in regulating coated pit dynamics revealed by small molecule inhibition. *Cell* **146**, 471–484 (2011).
18. Watanabe, S. et al. Clathrin regenerates synaptic vesicles from endosomes. *Nature* **515**, 228–233 (2014).
19. Jones, H. C. & Keep, R. F. Brain fluid calcium concentration and response to acute hypercalcaemia during development in the rat. *J. Physiol.* **402**, 579–593 (1988).
20. Hoppa, M. B., Gouzer, G., Armbruster, M. & Ryan, T. A. Control and plasticity of the presynaptic action potential waveform at small CNS nerve terminals. *Neuron* **84**, 778–789 (2014).
21. Rudolph, S., Tsai, M.-C., von Gersdorff, H. & Wadiche, J. I. The ubiquitous nature of multivesicular release. *Trends Neurosci.* **38**, 428–438 (2015).
22. Sakamoto, H. et al. Synaptic weight set by Munc13-1 supramolecular assemblies. *Nat. Neurosci.* **21**, 41–55 (2018).
23. Tang, A.-H. et al. A trans-synaptic nanocolumn aligns neurotransmitter release to receptors. *Nature* **536**, 210–214 (2016).
24. Hruska, M., Henderson, N., Le Marchand, S. J., Jafri, H. & Dalva, M. B. Synaptic nanomodules underlie the organization and plasticity of spine synapses. *Nat. Neurosci.* **21**, 671–682 (2018).
25. Dobrunz, L. E., Huang, E. P. & Stevens, C. F. Very short-term plasticity in hippocampal synapses. *Proc. Natl Acad. Sci. USA* **94**, 14843–14847 (1997).
26. Holderith, N. et al. Release probability of hippocampal glutamatergic terminals scales with the size of the active zone. *Nat. Neurosci.* **15**, 988–997 (2012).
27. Kaeser, P. S. & Regehr, W. G. Molecular mechanisms for synchronous, asynchronous, and spontaneous neurotransmitter release. *Annu. Rev. Physiol.* **76**, 333–363 (2014).
28. Grauel, M. K. et al. RIM-binding protein 2 regulates release probability by fine-tuning calcium channel localization at murine hippocampal synapses. *Proc. Natl Acad. Sci. USA* **113**, 11615–11620 (2016).
29. Adler, E., Augustine, J., Duffy, N. & Charlton, P. Alien intracellular calcium chelators attenuate release at the squid giant synapse. *J. Neurosci.* **11**, 1496–1507 (1991).
30. Chen, C. & Regehr, W. G. Contributions of residual calcium to fast synaptic transmission. *J. Neurosci.* **19**, 6257–6266 (1999).
31. Dittman, J. S. & Regehr, W. G. Calcium dependence and recovery kinetics of presynaptic depression at the climbing fiber to Purkinje cell synapse. *J. Neurosci.* **18**, 6147–6162 (1998).
32. Sakaba, T. & Neher, E. Calmodulin mediates rapid recruitment of fast-releasing synaptic vesicles at a calyx-type synapse. *Neuron* **32**, 1119–1131 (2001).
33. Redman, S. Quantal analysis of synaptic potentials in neurons of the central nervous system. *Physiol. Rev.* **70**, 165–198 (1990).
34. Tong, G. & Jahr, C. E. Multivesicular release from excitatory synapses of cultured hippocampal neurons. *Neuron* **12**, 51–59 (1994).
35. Auger, C., Kondo, S. & Marty, A. Multivesicular release at single functional synaptic sites in cerebellar stellate and basket cells. *J. Neurosci.* **18**, 4532–4547 (1998).
36. Balaji, J. & Ryan, T. A. Single-vesicle imaging reveals that synaptic vesicle exocytosis and endocytosis are coupled by a single stochastic mode. *Proc. Natl Acad. Sci. USA* **104**, 20576–20581 (2007).
37. Abenavoli, A. et al. Multimodal quantal release at individual hippocampal synapses: evidence for no lateral inhibition. *J. Neurosci.* **22**, 6336–6346 (2002).
38. Nakamura, Y. et al. Nanoscale distribution of presynaptic Ca^{2+} channels and its impact on vesicular release during development. *Neuron* **85**, 145–159 (2015).
39. Rebola, N. et al. Distinct nanoscale calcium channel and synaptic vesicle topographies contribute to the diversity of synaptic function. *Neuron* **104**, 693–710.e9 (2019).
40. Sabatini, B. L. & Regehr, W. G. Optical measurement of presynaptic calcium currents. *Biophys. J.* **74**, 1549–1563 (1998).
41. Raingo, J. et al. VAMP4 directs synaptic vesicles to a pool that selectively maintains asynchronous neurotransmission. *Nat. Neurosci.* **15**, 738–745 (2012).
42. Turecek, J. & Regehr, X. W. G. Synaptotagmin 7 mediates both facilitation and asynchronous release at granule cell synapses. *J. Neurosci.* **38**, 3240–3251 (2018).
43. Weber, J. P., Toft-Bertelsen, T. L., Mohrmann, R., Delgado-Martinez, I. & Sørensen, J. B. Synaptotagmin-7 is an asynchronous calcium sensor for synaptic transmission in neurons expressing SNAP-23. *PLoS ONE* **9**, e114033 (2014).
44. Yao, J., Gaffaney, J. D., Kwon, S. E. & Chapman, E. R. Doc2 is a Ca^{2+} sensor required for asynchronous neurotransmitter release. *Cell* **147**, 666–677 (2011).
45. Hu, Z., Tong, X. J. & Kaplan, J. M. UNC-13L, UNC-13S, and Tomosyn form a protein code for fast and slow neurotransmitter release in *Caenorhabditis elegans*. *eLife* **2013**, e00967 (2013).
46. Böhme, M. A. et al. Active zone scaffolds differentially accumulate Unc13 isoforms to tune Ca^{2+} channel–vesicle coupling. *Nat. Neurosci.* **19**, 1311–1320 (2016).
47. Clustering, C. C. et al. Bruchpilot promotes active zone assembly, Ca^{2+} channel clustering, and vesicle release. *Science* **312**, 1051–1054 (2006).
48. Lipstein, N. et al. Dynamic control of synaptic vesicle replenishment and short-term plasticity by Ca^{2+}–calmodulin–Munc13-1 signaling. *Neuron* **79**, 82–96 (2013).
49. Jackman, S. L., Turecek, J., Belinsky, J. E. & Regehr, W. G. The calcium sensor synaptotagmin 7 is required for synaptic facilitation. *Nature* **529**, 88–91 (2016).
50. Jackman, S. L. & Regehr, W. G. The mechanisms and functions of synaptic facilitation. *Neuron* **94**, 447–464 (2017).

Methods

All animal care was performed according to the National Institutes of Health guidelines for animal research with approval from the Animal Care and Use Committee at the Johns Hopkins University School of Medicine.

Neuronal cell culture. Cell cultures were prepared on 6-mm sapphire disks (Technotrade), mostly as previously described[7,18]. Newborn or embryonic day 18 C57/BL6J mice of both sexes were decapitated, followed by dissection of and transfer of brains to ice-cold HBSS. In the case of embryonic mice, heads were stored in HBSS on ice before dissection. For high-pressure freezing, neurons were cultured on a feeder layer of astrocytes. For FM dye experiments, astrocytes were grown on 22-mm coverslips for 1 week and placed on top of neurons cultured on sapphire disks with astrocytes facing neurons[51], with paraffin dots used as spacers. Astrocyte cultures were established from cortices trypsinized for 20 min at 37 °C with shaking, followed by trituration and seeding on T-75 flasks. Astrocytes were grown in DMEM medium supplemented with 10% fetal bovine serum and 0.1% penicillin–streptomycin for 2 weeks, then plated on poly-D-lysine-coated 6-mm sapphire disks atop glass coverslips in 12-well plates at a density of 50,000 cells per well to create a feeder layer. After 6 days, FUDR was added to stop cell division. The following morning, culture medium was replaced with neurobasal-A supplemented with 2% B27 and 0.1% penicillin–streptomycin (NB-A full medium, Invitrogen) before plating hippocampal neurons. Hippocampi were dissected and incubated in papain with shaking at 37 °C for 30–60 min, then triturated and plated on astrocytes at 50,000 or 75,000 cells per well. Before use, sapphire disks were carbon-coated with a "4" to indicate the side that cells are cultured on. The health of the cells, as indicated by de-adhered processes, floating dead cells and excessive clumping of cell bodies, was regularly assessed, as well as immediately before experiments. All experiments were performed between 13 and 17 days in vitro.

Electrical field stimulation. The electrical stimulator was manufactured by Leica to be compatible with the Leica ICE high-pressure freezer. The middle plate was designed as a circuit board trimmed to the dimensions of a standard Leica ICE high-pressure freezer middle plate. In the middle plate, there is a central 6-mm hole holding the sample sandwiched between two sapphire disks. This central hole was plated with two gold contact surfaces that are used to apply field stimulation to the sample. The standard spacer ring between the sapphire disks are conductive, and was replaced with nonconductive mylar rings of the same dimensions. The voltage applied to the sample was provided by a capacitor bank attached to the middle plate. The capacitors were charged just before the sample is loaded into the chamber. The current from the capacitors to the sample was controlled by a phototransistor. In the absence of light, there is no current passed from the capacitors to the sample contacts. In this way, the field stimulation can be activated within the chamber using the standard light stimulation function of the EM ICE.

FM dye uptake imaging and quantification. For the FM 1-43FX (Invitrogen) uptake assay, we used a modified version of a previously published protocol[52]. Neurons on sapphire disks were first incubated with Pitstop 2 (30 μM; Sigma) in physiological saline (1 mM Ca^{2+}) for 2 min. This treatment blocks the regeneration of synaptic vesicles from synaptic endosomes[18], which prevents FM dyes from being released during the washing procedure. Following the addition of FM dye (5 μg ml^{-1}), a sapphire disk was mounted on a middle plate, while another sapphire disk in the same well was left in the solution to ensure that both sapphire disks were incubated in FM dye for the same period of time. After charging the middle plate, 10 pulses of light (1 ms each) were applied at 20 Hz to discharge the capacitor and to induce 10 action potentials. Immediately after stimulation, both stimulated and unstimulated specimens were transferred to an 18-mm petri dish containing physiological saline solution (1 mM Ca^{2+}). FM dyes bound to the plasma membrane were washed off by passing current across the specimen using a transfer pipet for 1 min. Both samples were then transferred into warm (37 °C) PBS containing 4% paraformaldehyde and fixed for 30 min. After fixation, samples were washed three tims with PBS and immediately imaged on an Olympus IX81 epifluorescence microscope equipped with a Hamamatsu C9100-02 EMCCD camera run on SlideBook 6 with a mercury lamp illumination through a CFP/YFP filter set (Semrock) and a ×60, NA 1.4 Olympus UIS2 oil-immersion objective. For each condition, 7 images were acquired and 20 putative presynaptic terminals quantified, which were identified by their increased FM labeling relative to the rest of the axon, their shape and size by manual segmentation in ImageJ, and their total fluorescence intensity measured. Intensity values were then background corrected. All micrographs shown were acquired with the same settings on the microscope and later adjusted in brightness and contrast to the same degree in ImageJ, then rotated and cropped in Adobe Photoshop.

High-pressure freezing. Cells cultured on sapphire disks were frozen using an EM ICE high-pressure freezer (Leica Microsystems). The freezing apparatus was assembled on a table heated to 37 °C in a climate-control box, with all solutions pre-warmed (37 °C). Sapphire disks with neurons were carefully transferred from culture medium to a small culture dish containing physiological saline solution (140 mM NaCl, 2.4 mM KCl, 10 mM HEPES buffer, 10 mM glucose; pH adjusted to 7.3 with NaOH, 300 mOsm). NBQX (3 μM; Tocris) and bicuculline (30 μM; Tocris) were added to the physiological saline solution to block recurrent synaptic activity. $CaCl_2$ and $MgCl_2$ concentrations were 1.2 mM and 3.8 mM, respectively, except where indicated, in which case the $MgCl_2$ concentration was adjusted accordingly (3 mM $MgCl_2$ with 2 mM $CaCl_2$, 1 mM $MgCl_2$ with 4 mM $CaCl_2$). Cells were then fitted into the photoelectric middle plate. Filter paper was placed underneath the middle plate to remove all excess liquid. A mylar spacer ring was then placed atop the sapphire disk. To create a 'sandwich' of the solution described above, the underside of another sapphire disk was dipped in the solution so that some was held on by surface tension, then placed atop the spacer ring so that excess liquid again dispersed onto the filter paper. For voltage to be applied across the sample, it is essential for all components outside the sandwich to be dry, so the top of the sapphire and all other components of the setup were gently dried with another piece of filter paper. Finally, a rubber ring was added to hold everything in place. This entire assembly process took 3–5 min. The assembled middle plate was enclosed in two half cylinders then loaded into the freezing chamber, where the cells were stimulated for 1 ms before freezing at the desired time point, ranging from 5 ms to 105 ms. With this protocol, 10 V cm^{-1} is applied for 1 ms across a 6-mm space between the electrodes into which the sapphire disk fits, as confirmed by measurements from Leica. This field stimulation regimen in hippocampal cultures induces a single action potential and only negligibly depolarizes boutons directly[20]. Although action potentials could not be directly measured in this study, two pieces of data suggest that this device uniformly activates synapses. First, synapses across the field seem to take up FM dyes (Fig. 1). Second, roughly 35% of synapses responded to the stimulus, as determined by the presence of fusion pits after stimulation (Fig. 2). This fraction is consistent with the fraction of synapses that respond to an action potential, as determined using electrophysiology[53–55] and optical methods[56]. However, further study is necessary to assess the extent of action potential failure in neurons when this device is used.

For the EGTA experiments, the first half of the medium in which cells were grown was removed and set aside. EGTA-AM (Fisher) or DMSO was then added to the medium to a final concentration of 25 μM and 0.25% DMSO for 15 min to load the cells with EGTA. Cells were washed three times and left in the media that had been set aside for 15 min before freezing in the physiological saline solution described above (treatment protocol adapted from ref. [28]). For the TTX experiments, TTX was added to the freezing solution to a final concentration of 1 μM, and the cells were in TTX for 3–5 min before freezing.

Cooling rates during freezing were between 16,000 and 18,000 K s^{-1}. Membrane traffic stops at 0 °C, so the point at which the sample reaches this temperature can be considered the true time of freezing. On the EM ICE, we set the stimulation program to produce a 1-ms pulse, followed by a resting period (ranging from 0 ms to 10 s). By default, during the freeze process, the temperature sensor placed just outside the specimen chamber reaches 0 °C, which is precisely when the resting period of the stimulation program is complete. This causes an extra 5-ms delay in samples reaching 0 °C. Specifically, an additional ~4 ms is needed for the chamber to freeze (~3 ms faster than the HPM100) and another 1 ms for neurons to freeze[7]. Thus, a total of 5 ms delay is expected. This 5-ms delay was confirmed by direct measurements made by Leica Microsystems. Previous experiments indicated that this number may be off by ±1 ms due to the mechanics of the EM ICE[57]. Therefore, specimens were frozen, on average, 5 ms later than the time point programmed into the EM ICE, with relatively little variability. For example, to freeze at 5 or 8 ms, the delay period on the machine was set to "0 ms" or "3 ms". Thus, the time points indicated (5, 8, 11, 14 and 105 ms) are calculated based on this estimated 5-ms delay from the onset of stimulation.

Freeze substitution. After freezing, samples were transferred under liquid nitrogen to an EM AFS2 freeze substitution system at −90 °C (Leica Microsystems). Using pre-cooled tweezers, samples were quickly transferred to anhydrous acetone at −90 °C. After disassembling the freezing apparatus, sapphire disks with cells were quickly moved to cryovials containing 1% glutaraldehyde, 1% osmium tetroxide and 1% water in anhydrous acetone, which had been stored under liquid nitrogen then moved to the AFS2 system immediately before use. The freeze substitution program was as follows: −90 °C for 6–10 h (adjusted so that substitution would finish in the morning); 5 °C h^{-1} to −20 °C; 12 h at −20 °C; and 10 °C h^{-1} to 20 °C.

Embedding, sectioning and transmission electron microscopy. Samples in fixatives were washed three times, 10 min each, with anhydrous acetone, then stained en bloc with 1% uranyl acetate for 1 h with shaking. After three washes, samples were left in 30% epon araldite in anhydrous acetone for 3 h, then 70% epon araldite for 2 h, both with shaking. Samples were then transferred to caps of polyethylene BEEM capsules (EMS) and left in 90% epon araldite overnight at 4 °C. The next morning, samples were transferred to 100% epon araldite (epon, 6.2 g; araldite, 4.4 g; DDSA, 12.2 g; and BDMA, 0.8 ml) for 1 h, then again to 100% for 1 h, and finally transferred to 100% epon araldite and baked at 60 °C for 48 h.

For single-section imaging, 40-nm sections were cut, while 10–15 serial sections were cut for serial-section 3D reconstructions (50-nm thick in the first replicate and 40 nm in the second). Sections on single-slot grids coated with 0.7% pioloform were stained with 2.5% uranyl acetate then imaged at 80 kV on the ×93,000 setting on a Phillips CM 120 transmission electron microscope equipped with an AMT XR80 camera run on AMT Capture v.6. In some cases, including all

serial-section imaging, the microscopist was blinded to the different conditions, while in other cases they were not. To limit bias, synapses were found by bidirectional raster scanning along the section at ×93,000, which makes it difficult to pick certain synapses, as a synapse usually takes up most of this field of view. Synapses were identified by a vesicle-filled presynaptic bouton and a postsynaptic density. Postsynaptic densities are often subtle in our samples, but synaptic clefts were also identifiable by (1) their characteristic width, (2) the apposed membranes following each other closely and (3) vesicles near the presynaptic active zone. Only synapses with prominent postsynaptic densities were imaged for serial-sectioning reconstructions. About 125–150 micrographs per sample of anything that appeared to be a synapse were taken without close examination. For serial sectioning, at least 30 synapses per sample were imaged.

Electron microscopy image analysis. Images were annotated in a blinded manner, but not randomized in the initial time-course experiments (first replicate of data shown in Fig. 3) or in the first replicate of the serial-sectioning data in Fig. 2. For all other data, all the images from a single experiment were randomized for analysis as a single pool using a custom R (R Development Team) script. Only after this randomization process were images excluded from analysis, either because they appeared to not contain a bona fide synapse or the morphology was too poor for reliable annotation. This usually meant ~100 synapses per sample were analyzed for single sections. In some cases, membranes had low contrast against the cytoplasm, due mostly to good preservation of proteins in these tissues. These images are annotated after adjusting the contrast in ImageJ. The plasma membrane, active zone, docked synaptic vesicles, synaptic vesicles close to the active zone and pits (putative fusion events) were annotated in ImageJ using a custom plugin. The active zone was identified as the region of the presynaptic plasma membrane with the features described above for identifying a synapse. Docked vesicles were identified by their membrane appearing to be in contact with the plasma membrane at the active zone (0 nm from the plasma membrane); that is, there are no lighter pixels between the membranes. When comparing data, note that 'docking' is more narrowly defined in these data than in Imig et al.[4] (0–2 nm) and Chang et al.[9] (<5 nm), and is the definition of docking that we have used in previous publications[5,7,8]. Vesicles that were not manually annotated as docked, but were 0 nm away from the active zone plasma membrane, were automatically counted as docked when segmentation was quantitated (see below) for datasets counting the number of docked vesicles. Vesicles annotated as docked were automatically placed in the 0-nm bin of vesicle distances from the plasma membrane. Pits were identified as smooth curvature (not mirrored by the postsynaptic membrane) in an otherwise straight membrane. These pits are considered exocytic, as endocytic pits do not normally appear until 50 ms after an action potential[7], fluid phase markers are not internalized until ~100 ms[7] and ferritin-positive vesicles are not found near the active zone membrane until ~10 s after stimulation[18]. Pits lateral to the active zone are considered endocytic or membrane ruffles, since this is the primary site for ultrafast endocytosis[7]. Under these criteria, we could miss or over-annotate vesicles and pits. To minimize bias and to maintain consistency, all image segmentation, still in the form of randomized files, was thoroughly checked by a second member of the laboratory. For serial-section data, active zones with multiple pits were re-evaluated post hoc after unblinding to make sure they are not halves of the same structure. However, no corrections were made for synaptic vesicles, since vesicles are much more abundant and the same criteria were used to annotate them in all conditions. A similar amount of overestimate is expected in this case. Features were then quantitated using custom Matlab (MathWorks) scripts.

The location of pits and docked vesicles within the active zone from single sections was calculated from the distance from the center of the pit to the center and the edge of the active zone in a two-dimensional (2D) section. The distance from the center was normalized by dividing the distance to the edge by the half-width of the active zone. For 3D data, the distance to the center of the active zone was calculated from serial sections. First, the location in a 2D section was calculated as above. Then, the 3D distance was calculated to the center of the active zone in the middle section of the series using the Pythagorean theorem, with assumption that each section is the same thickness and the center of the active zone aligns in each image. Locations in 3D data were further corrected to be the density of vesicles/pits at each distance from the center of the active zone. This is because the total area for objects to be located increases with increasing distance from the center of a roughly circular object (for example, randomly distributed objects within a circular active zone would have a median distance from the center of 0.66, giving the impression that they are biased toward the edge: after calculating the density, this value would be 0.5). To calculate the density of vesicles/pits from the center to the edge in 3D reconstructions, the radial position of each vesicle/pit was converted to the fractional area of a circle bounded by that radius. In the case of a unit circle (the distance from the center to the edge is by definition 1, with the data normalized to the size of the active zone), this is simply the square of the original normalized distance to the center. The distance between pits and docked vesicles in different sections was approximated in a similar manner, where the edges of the hypothetical triangle are (1) the difference of the distances between each pit to the center of the active zone in each section and (2) the distance between the sections, again assuming a thickness of 50 nm.

The example micrographs shown were adjusted in brightness and contrast to different degrees (depending on the varying brightness and contrast of the raw images), rotated and cropped in Adobe Photoshop.

Statistical analysis. All data shown are pooled from multiple experiments (see Supplementary Table 2 for summary data for each replicate). All data were initially examined on a per-experiment basis (with all freezing done on the same day and all segmentation done in a single randomized batch), and none of the pooled data showed any result that was not found in each replicate individually. We did not predetermine sample sizes using power analysis, but based them ($N = 2–4$ independent cultures, $n > 200$ images) on our prior experience with flash-and-freeze data[7,8,18]. An alpha of 0.05 was used for statistical hypothesis testing. All data were tested for normality by D'Agostino–Pearson omnibus tests to determine whether parametric or nonparametric methods should be used. Comparisons between two groups were performed using a two-tailed Welch two-sample *t*-test or Wilcoxon rank-sum test. Comparisons between multiple groups followed by full pairwise comparisons were performed using one-way analysis of variance (ANOVA) followed by Tukey's honestly significant difference (HSD) test or Kruskal–Wallis test followed by Dunn's multiple comparisons test. Differences in the number of active zones containing at least one pit from active zone reconstructions in Fig. 2a were assessed using a chi-square test. For testing whether the locations of pits were biased toward the center or edge of the active zone, a two-tailed one-sample *t*-test or Wilcoxon rank-sum test with a theoretical median of 0.5 was used (each of these *P* values, as well as that of the comparisons between pit locations in different samples, were accordingly corrected for multiplicity using Bonferroni's method). All statistical analyses were performed and all graphs created in Graphpad Prism 6, 7 and 8.

Reporting Summary. Further information on research design is available in the Nature Research Reporting Summary linked to this article.

Data availability

Full data tables underlying the figures are available at https://figshare.com/authors/Shigeki_Watanabe/910686 and in the source data. Raw images and image analysis files are available upon request. Source data are provided with this paper.

Code availability

Custom R, Matlab and Fiji scripts are available at https://github.com/shigekiwatanabe/SynapsEM and are the subject of a manuscript currently in preparation.

References

51. Kaech, S. & Banker, G. Culturing hippocampal neurons. *Nat. Protoc.* **1**, 2406–2415 (2006).
52. Hoopmann, P., Rizzoli, S. O. & Betz, W. J. Imaging synaptic vesicle recycling by staining and destaining vesicles with FM dyes. *Cold Spring Harb. Protoc.* **7**, 77–83 (2012).
53. Allen, C. & Stevens, C. F. An evaluation of causes for unreliability of synaptic transmission. *Proc. Natl Acad. Sci. USA* **91**, 10380–10383 (1994).
54. Rosenmund, C., Clements, J. D. & Westbrook, G. L. Nonuniform probability of glutamate release at a hippocampal synapse. *Science* **262**, 754–757 (1993).
55. Hessler, N. A., Shirke, A. M. & Malinow, R. The probability of transmitter release at a mammalian central synapse. *Nature* **366**, 569–572 (1993).
56. Jensen, T. P. et al. Multiplex imaging relates quantal glutamate release to presynaptic Ca^{2+} homeostasis at multiple synapses in situ. *Nat. Commun.* **10**, 1414 (2019).
57. Watanabe, S. Flash-and-freeze: coordinating optogenetic stimulation with rapid freezing to visualize membrane dynamics at synapses with millisecond resolution. *Front. Synaptic Neurosci.* **8**, 24 (2016).

Acknowledgements

We are indebted to S. Li, Q. Gan, K. Itoh, D. Lubsanjav, C. Zhang and S. Markert for help with cell culture and freezing and for stimulating discussions. We also thank M. Delanoy and B. Smith for technical assistance with electron microscopy and K. T. DiNapoli for developing R code to randomize images. We thank P. Wurzinger and C. Tomova at Leica for the design and manufacture of the middle plate, M. A. Herman for initial tests of using a capacitor for field stimulation, H. Goldschmidt for help validating the stimulation device using pHluorin imaging, and N. Livingston for help with voltage imaging. We also thank the Marine Biological Laboratory and their neurobiology course for supporting the initial set of experiments (course supported by National Institutes of Health grant R25NS063307). S.W. and this work were supported by start-up funds from the Johns Hopkins University School of Medicine, Johns Hopkins Discovery funds and the National Science Foundation (1727260), and the National Institutes of Health (1DP2 NS111133-01 and 1R01 NS105810-01A1) awarded to S.W. S.W. is an Alfred P. Sloan fellow, a McKnight Foundation Scholar and a Klingenstein and Simons Foundation scholar. E.M.J. is an Investigator of the Howard Hughes Medical Institute. G.F.K. was supported by a grant from the National Institutes of Health to the Biochemistry, Cellular and Molecular

Biology program of the Johns Hopkins University School of Medicine (T32 GM007445) and is a National Science Foundation Graduate Research Fellow (2016217537). The EM ICE high-pressure freezer was purchased partly with funds from an equipment grant from the National Institutes of Health (S10RR026445) awarded to S. C. Kuo.

Author contributions

M.W.D., S.W. and E.M.J. conceived the zap-and-freeze technique. G.F.K. and S.W. designed the experiments and analyzed the data. S.W., G.F.K. and E.M.J. wrote the manuscript. G.F.K. performed all freezing experiments and single-section electron microscopy sample preparation, imaging and analyses, and FM dye uptake experiments, with technical assistance from S.W., with the exception of the first replicate of the 105-ms time point experiment (which was performed by S.W.) and the 1-s and 10-s time point experiments (which were performed by S.R.). M.C. and G.F.K. performed the serial sectioning 3D reconstruction electron microscopy imaging and analyses. S.W. and M.C. developed the Matlab code for image analyses. K.P.A., E.J.H., K.L., S.R. and T.V. performed pilot zap-and-freeze experiments and electron microscopy sample preparation, imaging and analyses. M.W.D. designed the prototype zap-and-freeze stimulation device. S.W. funded and oversaw the research.

Competing interests

The authors declare no competing interests.

Additional information

Extended data is available for this paper at https://doi.org/10.1038/s41593-020-00716-1.

Supplementary information is available for this paper at https://doi.org/10.1038/s41593-020-00716-1.

Correspondence and requests for materials should be addressed to S.W.

Peer review information *Nature Neuroscience* thanks Erwin Neher and the other, anonymous, reviewer(s) for their contribution to the peer review of this work.

Reprints and permissions information is available at www.nature.com/reprints.

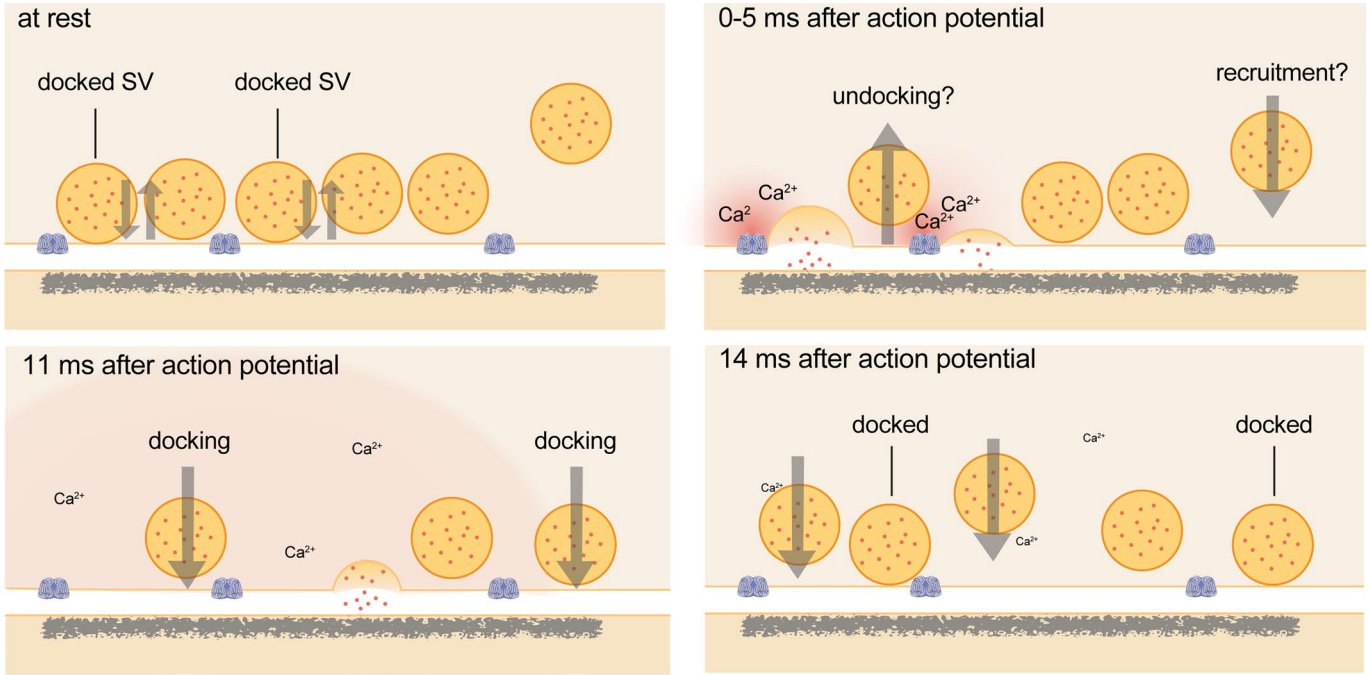

Extended Data Fig. 1 | Schematic of events at the active zone of a hippocampal bouton within the first 15 ms after an action potential. Vesicles close to the active zone are proposed to transit between docked and undocked states, with the on- and off-rates resulting in a certain number of vesicles docked and ready to fuse at any given time. Synchronous fusion, often of multiple vesicles, begins throughout the active zone within hundreds of microseconds, and the vesicles finish collapsing into the plasma membrane by 11 ms (note that the high local calcium shown only lasts ~100 microseconds). Between 5 and 11 ms, residual calcium triggers asynchronous fusion, preferentially toward the center of the active zone. Although shown here as taking place in the same active zone, the degree to which synchronous and asynchronous release may occur at the same active zone after a single action potential is unknown. By 14 ms, the vesicles from the peak of asynchronous fusion, which can continue for tens to hundreds of milliseconds, have fully collapsed into the plasma membrane, and new docked vesicles, which may start to be recruited in less than 10 ms, have fully replaced the vesicles used for fusion. These vesicles then undock or fuse within 100 ms. Whether these new vesicles dock at the same sites vacated by the fused vesicles, and whether newly docked vesicles contributed to synchronous and asynchronous fusion during the first 11 ms, remains to be tested.

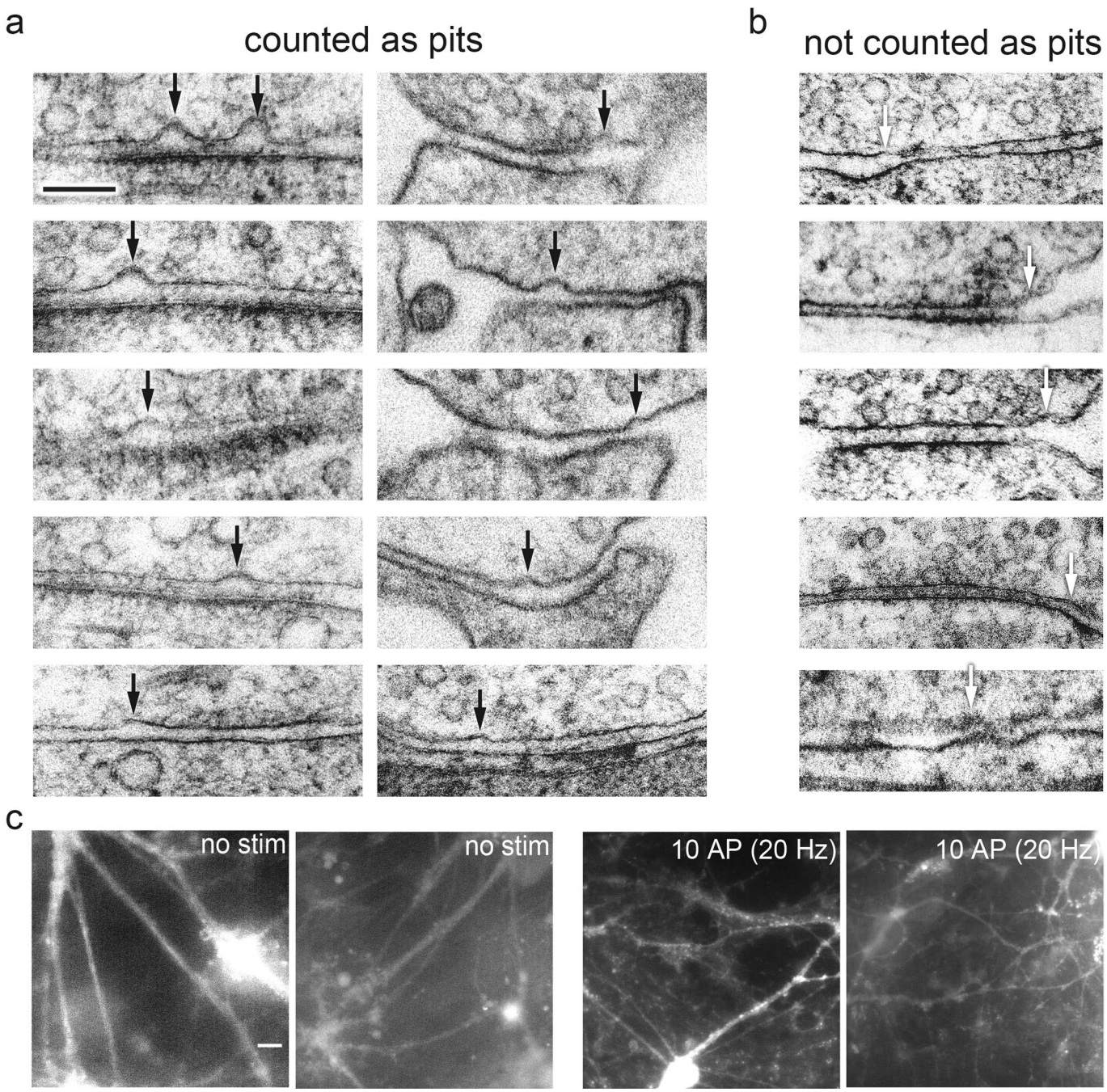

Extended Data Fig. 2 | Examples of pits in the active zone compared to pits outside the active zone or features not quantified as pits. a, Examples of pits in the active zone 5 ms after stimulation, indicated by black arrows. **b**, Examples of features not counted as pits, for instance because the curvature in the presynaptic membrane is mirrored by the postsynaptic membrane, indicated by white arrows. Scale bar: 100 nm **c**, Full fields-of-view of micrographs from the FM dye experiment described in Fig. 4b. Images from experiments described throughout the manuscript (N = 10 freezes from separate cultures on separate days). Cultured mouse hippocampal neurons were pre-incubated in 30 µM Pitstop 2 in physiological saline (1 mM Ca^{2+}) for 2 min, then either not stimulated or subjected to 10x 1 ms pulses at 20 Hz, at 37 °C in FM 1-43FX, followed by washing and fixation. Note that puncta along the processes became apparent after, suggesting that the zap-and-freeze device induces synaptic vesicle fusion and endocytosis. These images were collected randomly throughout the sapphire disks. Scale bar: 20 microns N = 1 experiment.

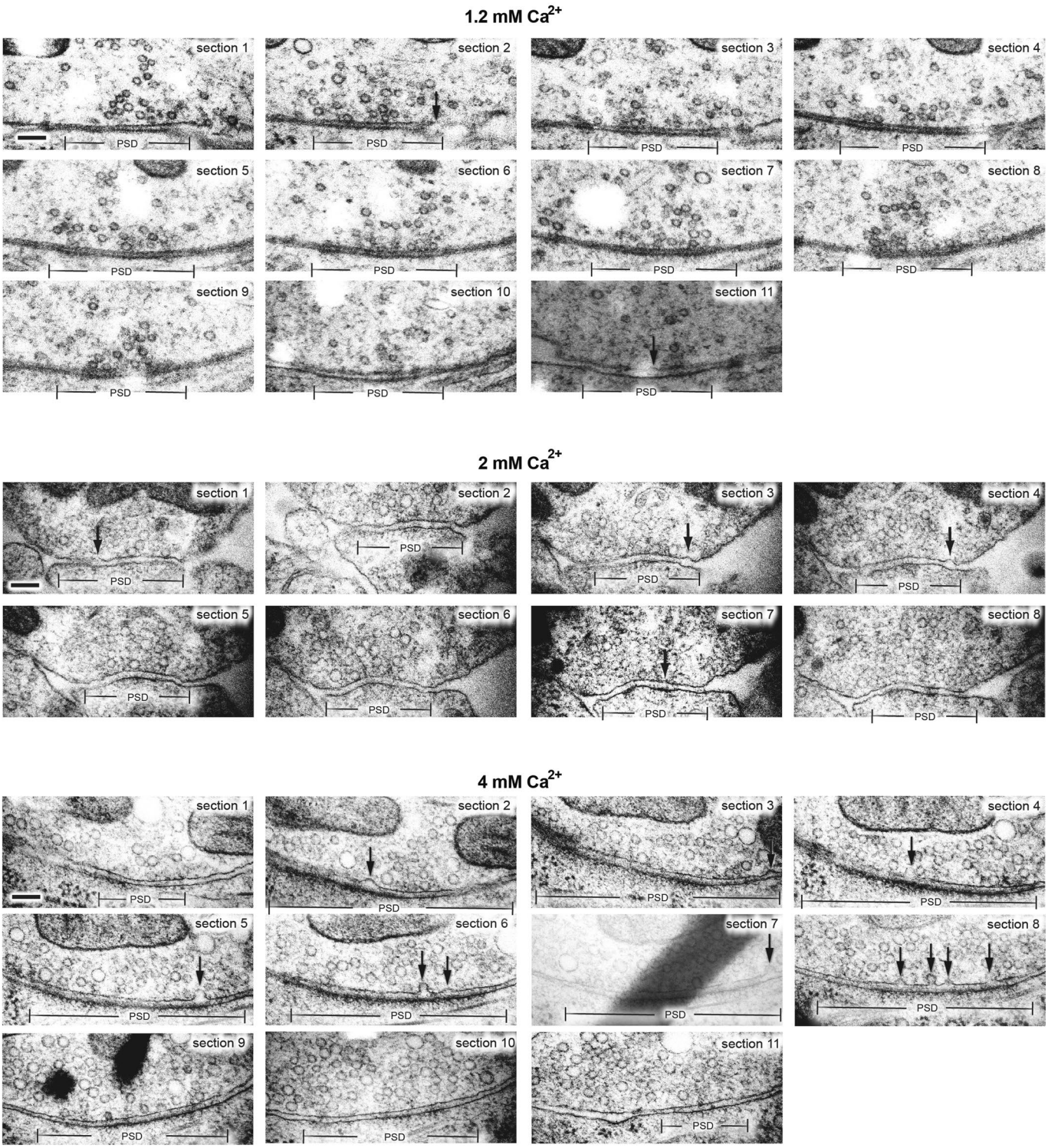

Extended Data Fig. 3 | Multiple fusion events in serial-sectioning reconstructions of active zones from neurons frozen 5 ms after an action potential. **a**, Example transmission electron micrographs from serial sections of active zones from neurons frozen 5 ms after an action potential in 1.2 mM, 2 mM, and 4 mM extracellular Ca^{2+} (from the same experiments described in Fig. 2). Scale bar: 100 nm. PSD: post-synaptic density. AP: action potential. Arrows indicate "pits" in the active zone (opposite the post-synaptic density), which are presumed to be vesicles fusing with the plasma membrane. Note that pits within the same active zone are often different depths. All data are from two experiments from separate cultures frozen on different days.; experiments in 1.2 mM Ca^{2+} were performed on separate days from a separate culture from the experiments in 2 mM and 4 mM Ca^{2+}.

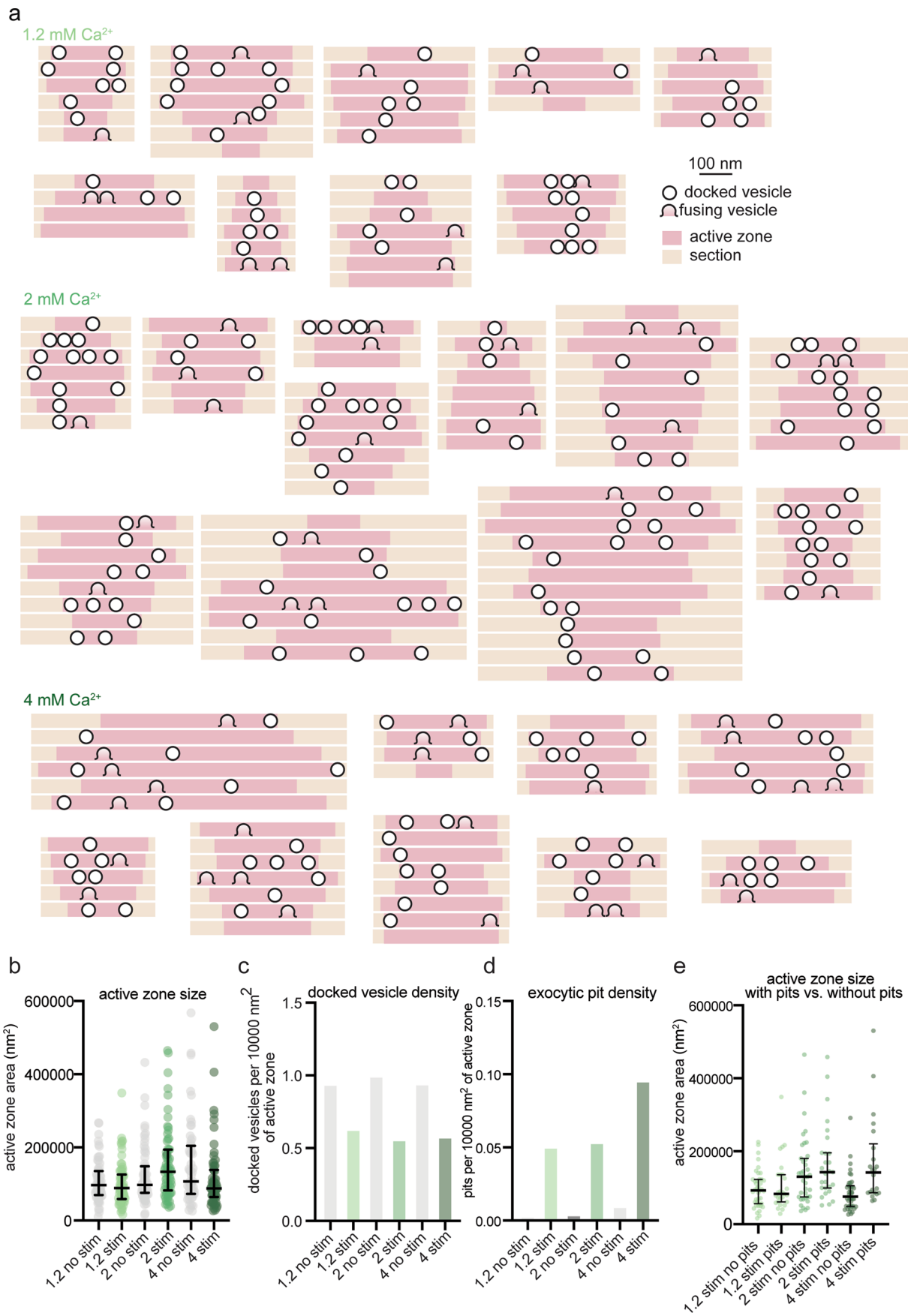

Extended Data Fig. 4 | See next page for caption.

Extended Data Fig. 4 | Representations of serial-sectioning reconstructions of active zones with exocytic pits. a, Graphical depictions of serial-sectioned active zones containing exocytic pits, from the experiments described in Fig. 2. **b**, Sizes of active zones from the data set shown in Fig. 2. Area was calculated as the product of the longest 2-D length of active zone in a 2-D profile from that synapse, the number of sections containing the active zone, and section thickness (that is, as the area of a rectangle). 1.2 mM, no stim, n = 62; 1.2 mM, stim, n = 68; 2 mM, no stim, n = 64; 2 mM, stim, n = 66; 4 mM, no stim, n = 65; 4 mM, stim, n = 64 reconstructed active zones. Error bars indicate median and interquartile range. **c**, Density of docked vesicles in the active zone, from the experiments shown in Fig. 2. Calculated as the total number of docked vesicles from a given sample x10000, divided by the sum of the total area of active zones from that sample. **d**, Density of exocytic pits in the active zone, from the experiments shown in Fig. 2. Calculated as the total number of pits from a given sample x10000, divided by the sum of the total area of active zones from that sample. **e**, Same data shown in **b**, sorted by whether the active zone contained an exocytic pit or not. See Supplementary Table 1 for full pairwise comparisons and summary statistics.

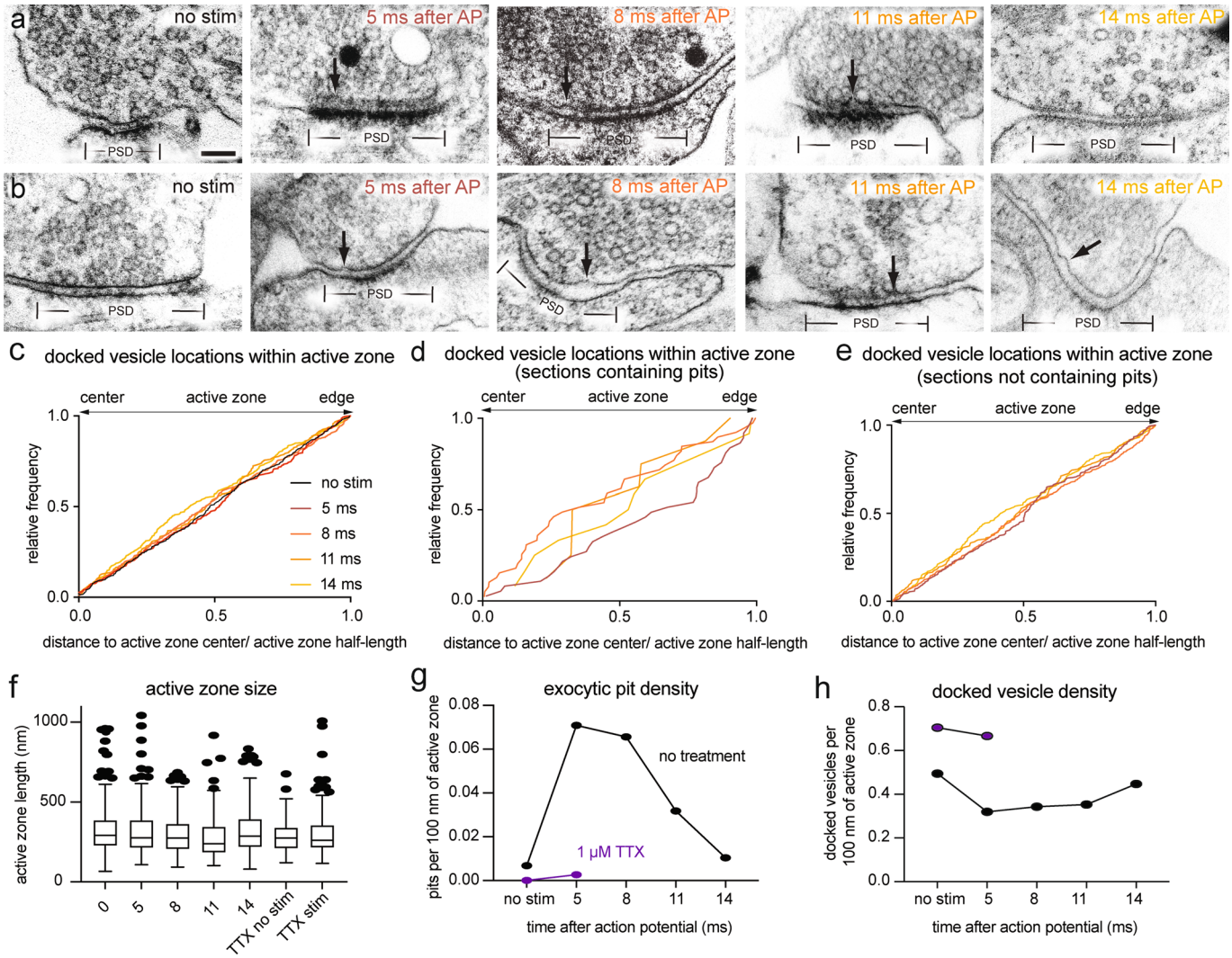

Extended Data Fig. 5 | Fusion intermediates at multiple time points during the first 14 ms after an action potential. a-b, Example transmission electron micrographs of synapses from neurons frozen without stimulation or 5, 8, 11, or 14 ms after an action potential (these are other examples from the same experiments shown in Fig. 3). **c**, Cumulative relative frequency of locations of docked vesicles within the active zone, normalized to the size of the active zone (no stim, n = 447; 5 ms, n = 300; 8 ms, n = 348; 11 ms, n = 188; 14 ms, n = 306 docked vesicles). **d**, Same data as in **c**, showing only vesicles from synaptic profiles that contain pits. **e**, Same data as in **c**, showing only vesicles from synaptic profiles that contain do not contain pits. **f**, Size of active zones from data in Fig. 3. Tukey boxplot shown; center: median, lower bound of box: 25th percentile, upper bound of box: 75th percentile, lower whisker: 25th percentile minus 1.5x interquartile range, upper whisker: 75th percentile plus 1.5x interquartile range; dots indicate values outside this range. No stim, n = 274; 5 ms, n = 315; 8 ms, n = 343; 11 ms, n = 192; 14 ms, n = 211; TTX, no stim, n = 121; and TTX, 5 ms, n = 255 synaptic profiles. **g**, Density of pits in the active zone, from the experiments shown in Fig. 3. Calculated as the total number of pits from a given sample x100, divided by the sum of the total length of active zones from that sample. **h**, Density of docked vesicles in the active zone, from the experiments shown in Fig. 3. Calculated as the total number of docked vesicles from a given sample x100, divided by the sum of the total length of active zones from that sample. Scale bar: 100 nm. PSD: post-synaptic density. AP: action potential. Arrows indicate "pits" in the active zone (opposite the post-synaptic density), which are presumed to be vesicles fusing with the plasma membrane. All data are from two experiments from separate cultures frozen on different days, except for the data from TTX treatment without stimulation, which are from a single experiment, and data from 5 and 8 ms, which are from three experiments. See Supplementary Table 1 for full pairwise comparisons and summary statistics.

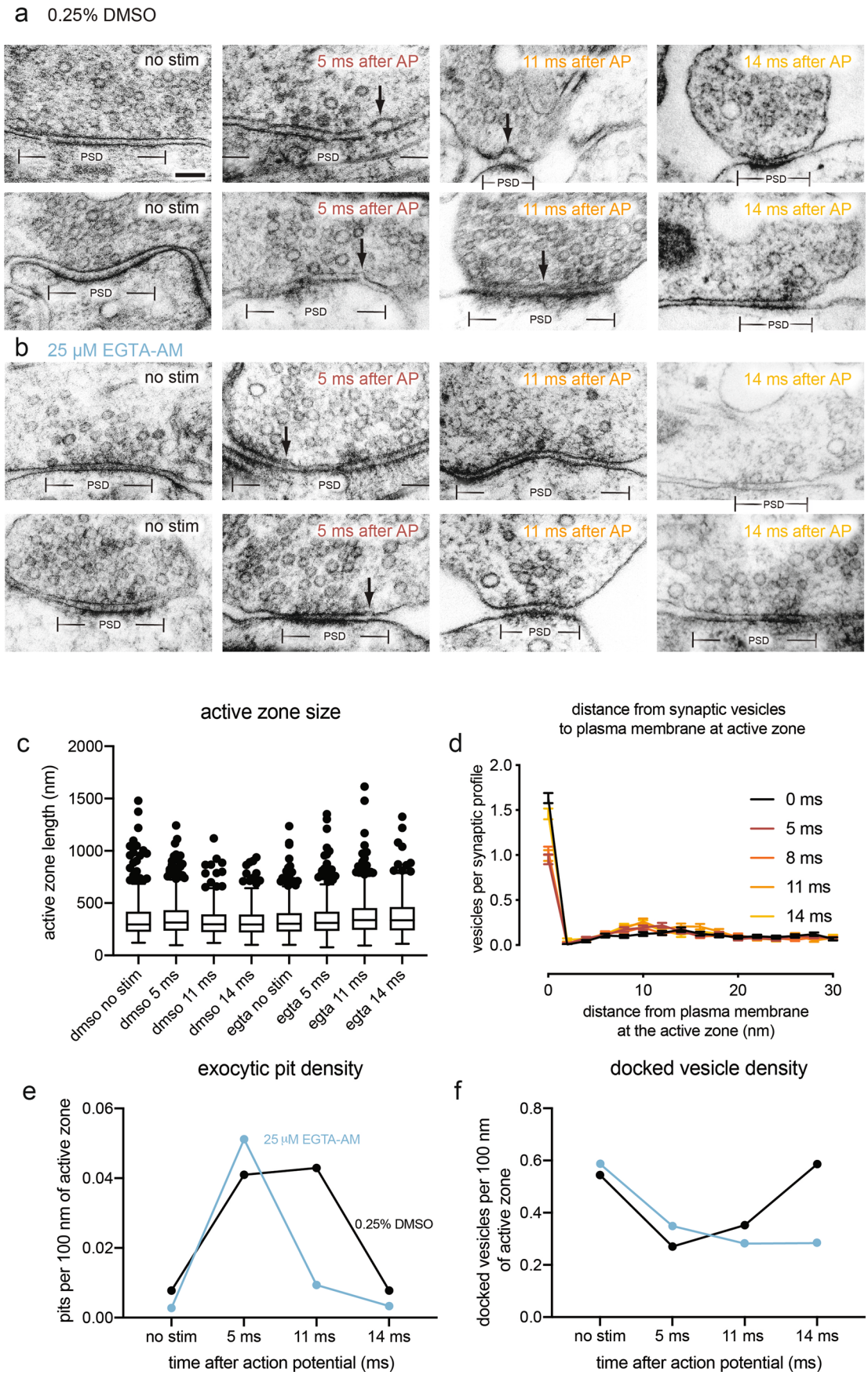

Extended Data Fig. 6 | See next page for caption.

Extended Data Fig. 6 | Chelating residual Ca^{2+} blocks fusion intermediates at 11 ms but not 5 ms after an action potential. a-b, Example transmission electron micrographs of synapses from neurons pre-treated with **a** 0.25% DMSO or **b** 25 μM EGTA-AM and frozen either without stimulation, 5 ms after stimulation, or 11 ms after stimulation (these are other examples from the same experiments shown in Fig. 4). Scale bar: 100 nm. PSD: post-synaptic density. AP: action potential. Arrows indicate "pits" in the active zone (opposite the post-synaptic density), which are presumed to be vesicles fusing with the plasma membrane. **c**, Size of active zones from data in Fig. 4. Tukey boxplot shown; center: median, lower bound of box: 25th percentile, upper bound of box: 75th percentile, lower whisker: 25th percentile minus 1.5x interquartile range, upper whisker: 75th percentile plus 1.5x interquartile range; dots indicate values outside this range. See Supplementary Table 1 for full pairwise comparisons and summary statistics. **d**, Distances of synaptic vesicles from the plasma membrane at the active zone, including both vesicles that were annotated as docked and not docked, from data in Fig. 3. No stim, n = 274; 5 ms, n = 315; 8 ms, n = 343; 11 ms, n = 192; 14 ms, n = 211; TTX, no stim, n = 121; and TTX, 5 ms, n = 255 synaptic profiles. Distances are binned in 2-nm increments, except for "0", which indicates vesicles ~0 nm from the active zone membrane ("2" indicates vesicles 0.1-2 nm from the membrane, "4" indicates 3-4 nm, etc.). Error bars indicate standard error of the mean. **e**, Number of pits in the active zone per 100 nm of active zone, from data in Fig. 4. **f**, Number of docked per 100 nm of active zone, from data in Fig. 4. All data from the experiments described in Fig. 4 are from 4 experiments for no stim and 5 ms time points, 3 experiments for 11 ms, and 2 experiments for 14 ms, from separate cultures frozen on different days (See Supplementary Table 2 for count data from each experiment).

nature research

Corresponding author(s): Shigeki Watanabe

Last updated by author(s): Jul 10, 2020

Reporting Summary

Nature Research wishes to improve the reproducibility of the work that we publish. This form provides structure for consistency and transparency in reporting. For further information on Nature Research policies, see our Editorial Policies and the Editorial Policy Checklist.

Statistics

For all statistical analyses, confirm that the following items are present in the figure legend, table legend, main text, or Methods section.

n/a	Confirmed	
☐	☒	The exact sample size (*n*) for each experimental group/condition, given as a discrete number and unit of measurement
☐	☒	A statement on whether measurements were taken from distinct samples or whether the same sample was measured repeatedly
☐	☒	The statistical test(s) used AND whether they are one- or two-sided *Only common tests should be described solely by name; describe more complex techniques in the Methods section.*
☐	☒	A description of all covariates tested
☐	☒	A description of any assumptions or corrections, such as tests of normality and adjustment for multiple comparisons
☐	☒	A full description of the statistical parameters including central tendency (e.g. means) or other basic estimates (e.g. regression coefficient) AND variation (e.g. standard deviation) or associated estimates of uncertainty (e.g. confidence intervals)
☐	☒	For null hypothesis testing, the test statistic (e.g. *F*, *t*, *r*) with confidence intervals, effect sizes, degrees of freedom and *P* value noted *Give P values as exact values whenever suitable.*
☒	☐	For Bayesian analysis, information on the choice of priors and Markov chain Monte Carlo settings
☒	☐	For hierarchical and complex designs, identification of the appropriate level for tests and full reporting of outcomes
☒	☐	Estimates of effect sizes (e.g. Cohen's *d*, Pearson's *r*), indicating how they were calculated

Our web collection on statistics for biologists contains articles on many of the points above.

Software and code

Policy information about availability of computer code

Data collection	The light microscopy camera was run on SlideBook 6. The electron microscopy camera was run on AMT Capture v6
Data analysis	The electron microscopy images were randomized using a custom R script (R Studio 1.3, R version 3.5.1). Features were manually segmented in Fiji (version 1.0) using a custom plugin. Features were quantified in MATLAB versions R2017-R2020a using custom scripts. Statistical analysis and data visualization were performed in GraphPad Prism 6, 7, and 8. Custom R, MATLAB, and Fiji scripts are available upon request, and are the subject of a manuscript currently in preparation.

For manuscripts utilizing custom algorithms or software that are central to the research but not yet described in published literature, software must be made available to editors and reviewers. We strongly encourage code deposition in a community repository (e.g. GitHub). See the Nature Research guidelines for submitting code & software for further information.

Data

Policy information about availability of data

All manuscripts must include a data availability statement. This statement should provide the following information, where applicable:

- Accession codes, unique identifiers, or web links for publicly available datasets
- A list of figures that have associated raw data
- A description of any restrictions on data availability

Full data tables underlying the figures are available at https://figshare.com/authors/Shigeki_Watanabe/9106865 and in the Source Data. Raw images and image analysis files are available upon request.

Field-specific reporting

Please select the one below that is the best fit for your research. If you are not sure, read the appropriate sections before making your selection.

☒ Life sciences ☐ Behavioural & social sciences ☐ Ecological, evolutionary & environmental sciences

For a reference copy of the document with all sections, see nature.com/documents/nr-reporting-summary-flat.pdf

Life sciences study design

All studies must disclose on these points even when the disclosure is negative.

Sample size	Power analysis was not used to determine the number (n) of synaptic profiles (2D EM) or serial-sectioning reconstructed active zones (3D EM). Our threshold of n >200 (from N = 2 or more experiments) for synaptic profiles was taken from previous work (Watanabe et al., 2013), based on 15-20% of synapses containing endocytic or exocytic events, such that >30 synapses with endocytic or exocytic events would be captured. For 3D EM, at least 30 active zones for each condition were reconstructed so that at least ~10 synapses with fusion events would be captured per replicate (based on prior data that ~30% of synapses respond to an action potential; Watanabe et al., 2013).
Data exclusions	Images that could not be reliably segmented, either because the image was not of a bona fide synapse or morphology was too poor, were excluded from segmentation; this was done only after randomizing the images. No other data were excluded.
Replication	All experiments were performed at least twice, and in most cases three times (from separate litters, different rounds of neuronal cell culture, frozen and processed separately, and segmented in separate batches of randomized images). While statistical analysis was performed on the data from all experiments pooled together, in each case similar results were obtained in each experiment. Furthermore, the DMSO controls shown in Figure 4 effectively serve as replicates of the no-stim, 5, and 11 ms time points from the experiments in Figure 3, and similar results were obtained for all metrics, except that 1) the number of pits at the 11 ms time point was greater in the DMSO controls and 2) fusions at 11 ms were concentrated at the center of the active zone in the DMSO controls as in the other experiments, but not as strongly, and 3) the number of docked vesicles was greater, though the proportional difference between the no-stim control and stimulated samples was similar.
Randomization	No randomization into experimental groups was performed prior to freezing, as different wells of the cell culture dish were presumed identical prior to handling during the experiment. For image segmentations, images were always randomized before manual segmentation, except for 2 (out of N = 3) of the experiments shown in Figure 3 and the first replicate of the experiments show in Figure 2, in which case they were analyzed blind by a person who was not familiar with the design of the experiment. These were the earliest experiments, and we had not yet adopted randomization scripts for our images.
Blinding	In the first two (of N = 3) experiments in Figure 3, all serial-section imaging (Figure 2), and two of the replicates of the experiments described in Figure 4 and 5, the microscopist was blind to the different conditions, while in all other cases they were not. To limit bias, synapses were found by bidirectional raster scanning along the section at 93,000x, which makes it difficult to "pick" certain synapses, as a synapse usually takes up most of this field of view, and anything that appeared to be a synapse was imaged without close examination. Because features identified were subtle, and any visible synapse was imaged, the possibility for bias during imaging is limited, even without blinding. For all other aspects of the study, blinding is not applicable. Blinding or group allocation was not possible while freezing samples, as all differences between treatment groups (EGTA treatment, stimulation/time point) were performed during the experiments.

Reporting for specific materials, systems and methods

We require information from authors about some types of materials, experimental systems and methods used in many studies. Here, indicate whether each material, system or method listed is relevant to your study. If you are not sure if a list item applies to your research, read the appropriate section before selecting a response.

Materials & experimental systems

n/a	Involved in the study
☒	☐ Antibodies
☒	☐ Eukaryotic cell lines
☒	☐ Palaeontology and archaeology
☐	☒ Animals and other organisms
☒	☐ Human research participants
☒	☐ Clinical data
☒	☐ Dual use research of concern

Methods

n/a	Involved in the study
☒	☐ ChIP-seq
☒	☐ Flow cytometry
☒	☐ MRI-based neuroimaging

Animals and other organisms

Policy information about studies involving animals; ARRIVE guidelines recommended for reporting animal research

Laboratory animals	No experiments were performed using live animals, only primary cell cultures. E18 or P0 wild-type C57BL/6J mice of both sexes were used for all cell culture. The sex of newborn or embryonic pups cannot be identified, but cells for neuronal culture were pooled from

	all the mice in a litter, and so contained cells from mice of both sexes in each experiment.
Wild animals	This study did not involve wild animals
Field-collected samples	This study did not involve samples collected from the field.
Ethics oversight	All animal care was performed according to the National Institutes of Health guidelines for animal research with approval from the Animal Care and Use Committee at the Johns Hopkins University School of Medicine.

Note that full information on the approval of the study protocol must also be provided in the manuscript.